Research Square

Preprints are preliminary reports that have not undergone peer review.
They should not be considered conclusive, used to inform clinical practice,
or referenced by the media as validated information.

Morphological and chemical characterization of wooden nails and matrix after nail insertion

Hans Korte
DR. HANS KORTE Wood & Fibres Innovation Consulting
Sergej Kaschuro
Thuenen
Gerald Koch
Thuenen
Daniela Paul
Thuenen
Jens Berger
Universität Hamburg
Anna Harima
Universität Hamburg
Katrin Schwarz
Universität Hamburg
Bodo Saake
Universität Hamburg
Stefan Siemers
Beck Engineering GmbH & Co. KG
Sylvia Diestel
Sylvia.Diestel@Thuenen.de

Thuenen

Research Article

Keywords: wooden nails, LignoLoc, densification, cracks, molten layers, lignin adhesion, X-ray computed microtomography (CT)

Posted Date: November 17th, 2026

DOI: https://doi.org/10.21203/rs.3.rs-11522062/v1

License: This work is licensed under a Creative Commons Attribution 4.0 International License.
Read Full License

Additional Declarations: Competing interest reported. Financial interests: Author SS is employee of BECK Engineereing GmbH & Co. KG, 5270 Mauerkirchen, Austria. Author HK is consultant to BECK Fastening GmbH.

Morphological and chemical characterization of wooden nails and matrix after nail insertion

Hans Korte[1], Sergej Kaschuro[2], Gerald Koch[2], Daniela Paul[2], Jens Berger[3], Anna Harima[3], Katrin Schwarz[3], Bodo Saake[3], Stefan Siemers[4], Sylvia Diestel[2]

[1]DR. HANS KORTE Wood & Fibres Innovation Consulting, Breite Str. 52, 23966 Wismar, Germany, e-mail: korte@hanskorte.de, Tel. +49 177 7859440, ORCID ID: 0000-0003-0744-8476
[2]Thuenen, Institute of Wood Research, Hamburg, Germany. Sylvia.Diestel@Thuenen.de, ORCID ID: 0000-0003-3190-4793, Gerald.koch@thuenen.de, ORCID ID 0000-0001-9409-5650
[3]University of Hamburg, Institute of Wood Science, Hamburg, Germany, Jens Berger ORCID ID 0009-0002-5212-9634
[4]Beck Engineering GmbH & Co. KG, Mauerkirchen, Austria

Abstract

This study examines the morphological and chemical characteristics of wooden nails and the surrounding spruce matrix when driven in at high speed. The aim is to improve understanding of the structural changes and chemical processes that occur in the contact zone between the nail and the matrix. Using X-ray computed microtomography and high-resolution reflected light microscopy, distinct zones of compaction running parallel to the nail shaft are identified that abruptly transitioned into uncompacted material. Cracking in the matrix was primarily caused by splitting, as well as by tensile forces running parallel to the grain. Based on these findings, a new nail tip with cutting edges was developed. This significantly reduces cracking forces and minimises the distance required for crack prevention between the nail and the edge. Chemical analyses using size exclusion chromatography, pyrolysis gas chromatography/mass spectrometry, and ultraviolet microspectrophotometry contradicted the hypothesis of a continuous layer of molten lignin as occurs in wood welding. Although temperatures of around 200 °C are briefly reached during driving, this duration of a few milliseconds is insufficient for polysaccharide degradation. Instead, the thermally induced modification and cross-linking of the lignin in the boundary zone is more likely. Evidence for this includes an increase in molecular weight, changes to the lignin side chains, and greater UV absorption.
In summary, the study shows that the bond between the wooden nail and the matrix is based primarily on mechanical compaction and the specific chemical modification of lignin, rather than the formation of conventional thermal degradation products.

Keywords: wooden nails, LignoLoc, densification, cracks, molten layers, lignin adhesion, X-ray computed microtomography (CT)

1 Introduction

The first publication on wooden nails that could be driven directly into wood and wood-based materials without the need for pre-drilling when using a pneumatic nailer appeared in 2018 (Korte, et al., 2018). Since then, other authors have investigated various aspects of this technology, including the bonding mechanism (Korte, et al., 2026; Wang, et al., 2025; Han, et al., 2023; Fan, et al., 2025) the strength of wooden constructions (Bergsagel, et al., 2025; Giordano, 2020; Han, et al. 2023; Hasan, et al., 2019; Khan, et al., 2025; Ruan, et al. 2022; Wang, et al. 2025; Wang, et al. 2025; Zhang, et al. 2026; Bruzzone, et al. 2026, Crovella, et al., 2025), the environmental impact (Bucklin, et al., 2023; Heisel, et al. 2025; Zhang, et al., 2026) and combinations of these areas of research.
When nails are driven or shot into a wooden matrix, the surrounding wood is displaced in the direction of driving and across it. This displaced material appears as two opposing compaction zones along the nail shaft. The cell layers (e.g. softwood's early and late wood in the compression zone) have a bent orientation in the direction of the shot. Cracks appear in front of the tip and along the grain in the vicinity of the nail (Korte, et al. 2018; Wang, et al. 2025).
During high-speed nail insertion (30–50 ms^{-1}) heat is generated on the surface, reaching approximately 200 °C (Korte, et al. 2026). The nail bonds with the matrix, doubling the pull-out strength compared to a steel nail of the same dimensions (Korte et al., 2018). Wang, et al. (2025) found an almost threefold increase in the characteristic pull-out strength of shot-in nails compared to nails driven-in slowly. Some researchers (Han, et al., 2023; Wang, et al., 2025) conclude that the increased pull-out strength of shot-in wooden nails indicates the presence of a layer of melted and re-solidified lignin in the contact zone between the nail and the matrix.

If it exists, such a layer should be comparable to the layers detected in wood welding (Suthoff, et al. 1996; Pizzi, et al., 2004; Stamm, et al. 2005; Gfeller; et al. 2003). In wood welding temperatures of up to 450 °C are generated over several seconds (Stamm, et al., 2005). When Norway spruce (*Picea abies*) is welded, it are mainly the polysaccharides that break down (Stamm, et al., 2006). However, temperatures generated on the surface of nails during the insertion process into wood only reach around 200 °C for a few milliseconds (Korte, et al. 2026). Therefore it is questionable whether these significantly milder conditions (a lower temperature over a much shorter period of time) are sufficient to break down polysaccharides or lignin.
This publication examines morphological changes in wood nails and the wood matrix after insertion, the chemical composition of the contact area between the nail and matrix, and crack formation in the wood matrix. Understanding the reasons for crack formation has led to improvements in nail tip design, reducing and/or modifying crack formation.

2 Material and methods

2.1 Sample preparation

In addition to nails made from wood composites (LignoLoc® made from Compreg), nails made from solid beech (*Fagus sylvatica* L.) and hornbeam (*Carpinus betulus* L.) were used. Nail diameters were 2.8 mm, 3.7 mm, 4.7 mm and 5.3 mm and the angles of the two flanks of a tip varied from 30°, 60° to 90°. Wooden matrix material to nail in was Norway spruce (*Picea abies* (L.) H. Karst). The method of insertion is described by Korte et al. (2026). Preparation for microscopy and scanning UV-microspectrophotometry (UMSP) is according to Korte et al. 2018. For X-ray computer microtomography (CT) analysis, cylindrical spruce samples with a diameter of 40 mm and a grain direction perpendicular to the cylinder axis were wrapped with rayon fabric tapes impregnated with PVA glue (Ponal wasserfest, Henkel, Düsseldorf, Germany), and the surface was also covered. After drying, the tight wrap stabilises the cylinder against total cracking when nails are inserted. Most nails were inserted in a radial direction, perpendicular to the surface.

2.2 X-ray computer microtomography

Most CT scans were performed at the European Synchrotron Radiation Facility (ESRF) in Grenoble, France. The detector-to-sample distance was 2000 mm and the energy was 152 keV. Samples were scanned in BM18 (a beamline for hierarchical phase-contrast tomography) at a resolution of 4.01 µm, with 2–3 images taken per sample. The scans were reconstructed at the ESRF, with the images merged along the nail direction. Visualisation and evaluation were performed using Avizo® (Thermo Fisher Scientific, Waltham, MA, USA), ImageJ and Fiji software at Thünen. The sample in Fig. 9 was analysed at Thünen with a voxel resolution of 38 µm on a CT-ALPHA (ProCon X-Ray GmbH, Sarstedt, Germany).

2.3 Microscopy

Structural changes in the wooden tissue and the wooden nails were characterized by high-resolution reflected-light microscopy using a VHX-7000 digital microscope (KEYENCE, Japan) and an SZX16 stereomicroscope (OLYMPUS, Japan). For the microscopic examination, the wood surfaces were carefully prepared by gentle polishing to obtain smooth surfaces while minimizing preparation-induced alterations of the wood microstructure. High-resolution micrographs were acquired at the interfaces between the wood tissue and the wooden nails to evaluate the microstructural characteristics and structural modifications associated with the joining process.

2.4 Sample preparation of nail layers

In order to investigate the chemical components of the material in the contact zone between the nail and the matrix, LignoLoc, beech and hornbeam nails were shot into spruce square timber. The timbers were then cut into cubes, which were split along the plane of the nails using a wood chisel. Nails with fibres adhering to them were recovered from the fracture surfaces. These nails then were repeatedly passed through perforated stainless-steel templates with decreasing 0.1 mm diameter holes, and the resulting fibres that were skimmed off were collected in separate fractions according to their hole diameter. The fractions of several nails then were combined to obtain sufficient material for the extraction.

2.5 Extraction

The separated nail layer fractions were extracted with acetone-water (v/v 9:1). Therefore 940 µl of acetone-water were added to 60 mg of the wood in a sealed vial and extracted for 24 h at 55 °C in an Eppendorf Thermomixer (Eppendorf SE, Hamburg, Germany) at 885 rpm and then filtered. These extracts were numbered with the prefix N (e.g N1, N2, …). The filtrate then was analyzed by size exclusion chromatography (SEC) and pyrolysis gas chromatography/mass spectrometry (Py-GC/MS).

2.6 Size exclusion chromatography

For SEC of acetone:water extracts, the extract samples were dried and re-dissolved in the eluent. Chromatography was performed using two PolarGel-M columns (300 x 7.5 mm) (Agilent, Santa Clara, CA, USA) in series, along with a PolarGel-M guard column (50 x 7.5 mm). The eluent was dimethyl sulfoxide containing 0.1% lithium bromide (LiBr).

Calibration was performed using polyethylene glycol as the standard, with refractive index (RI) and ultraviolet (UV) detection at 280 nm (Schütt, et al., 2013).

2.7 Pyrolysis-GC/MS

For Py-GC/MS analysis the extracts were applied to the pyrolysis cups by evaporating the solvents of the applied extract solutions. This process was repeated with adjusted volumes until the desired dry mass of 95 ± 5 µg per pyrolysis cup was obtained. After that, the sample cups were introduced into the pyrolysis system for analysis.

Py-GC/MS analysis was carried out in a Frontier-Lab Micro-furnace Double-Shot Pyrolyzer (Py-2020iD) equipped with an Autosampler (AS-1020 E, Frontier Laboratories Ltd., Fukushima, Japan). The temperature for pyrolysis was set at 500 °C and the pyrolysis interface temperature at 330 °C. The inlet and the GC/MS interface temperature were kept at 320 °C. Helium was used as a carrier gas for pyrolysis and gas chromatographic separation. The split ratio was set to 30:1 and a flow rate of 1 ml/min was set for gas chromatographic separation using a ZB-5HT (7HG-G015-11, Phenomenex Inc., Torrance, Ca., USA) fused silica capillary column.

The GC oven program starts with 4 min at 45 °C, changes to 5 °Cmin^{-1} up to 340 °C and kept 15 min at 340 °C. Mass spectra were determined by an Agilent 5973 inert MSD (Santa Clara, Ca., USA) with 70 eV electron impact ionization energy. Scan range was 15–550 mz^{-1} with a threshold of 150.

Evaluation was performed using OpenChrome© (vers. 1.4.0.202202150904, Lablicate GmbH, Hamburg, Germany). Data processing includes rounding of the ions (mz^{-1}), signal smoothing with Savitzky-Golay (Savitzky, et al., 1964), peak detection and deconvolution by multivariate curve resolution – alternating regression (MCR-AR Targeted Chained) and integration with trapezoid integrator in the retention time range 10–40 min. For the determination of the guaiacyl (G), syringyl (S), p-hydroxyphenol (H) lignin pyrolysis products, the peaks were identified by the "Lignin (SGH) and Carbohydrate (C)" peak identifier (Gerber, et al., 2012) and NIST 20 database (National Institute of Standards and Technology, Gaithersburg, MD, USA).

The G-lignin pyrolysis products then were classified by length of their side chain in two groups. Short side chain G-lignin building blocks (G-SC) with 1–2 carbon atoms attached to the aromatic ring including guaiacol and long side chain G-lignin building blocks (G-LC) with more than 2 aliphatic carbon atoms at the aromatic ring (Fig. 11). Oxidized side chains were excluded. The G-SC to G-LC ratio was determined from the peak area sums of the G-SC and the G-LC pyrolysis products. The total peak area of the G-lignin building blocks (∑G) includes the G-SC and G-LC, as well as the oxidized side chains.

3 Results and discussion

3.1 Morphological characterization

When nails are driven into solid wood, they are typically inserted at an angle between 0° and 90° relative to the grain, but very seldom in the longitudinal direction, because solid wood is most susceptible to cracking in this direction. Softwood has a tensile strength of 2–10% in the tangential direction and 3–25% in the radial direction compared to the longitudinal direction (Kollmann, 1951; Niemz, et al. 2023). In the radial direction, the nail tip passes through the thin-walled early wood and thick-walled late wood layers, which are perpendicular to the longitudinal direction.

During nail insertion, the surrounding wood is displaced in all three principal directions - radial (R), tangential (T) and longitudinal (L) - but the magnitude and manner of the displacement differs for each direction and between different wood structures. Figure 1 shows a LignoLoc nail that has been driven into spruce wood and prepared for analysis in the R/T plane.

The individual image sections can be interpreted as the frozen state of the driving process. Deformation of the individual annual rings illustrates what happens during insertion. The lowest annual ring (number 1 in Fig. 1) is not intersected by the nail but is slightly deformed downward, with a small crack at nail-tip level. The annual ring above (#2) is clearly indented in the direction of the shot. The nail tip separates it into two parts. The early wood layer between the two late wood sections #1 and #2 is subjected to compression and appears darker than the adjacent early- wood on either side. The lateral extension of the combined compression zones in the T-direction is approximately equal to the width of the nail.

The flanks of the nail tips form an angle of approximately 60° and push the annual rings aside. The annual rings can break into individual clods, as can clearly be seen in annual ring #4. Once the flanks have passed an annual ring – in Figure 1, this occurs from annual ring #4 onwards - on both sides a compacted zone develops parallel to the nail. Compaction is mostly pronounced in the early-wood; the adjacent late-wood remains essentially unchanged. The annual rings, separated by the LignoLoc nail, bend from their original shape in the direction of the shot. The compacted zone terminates approximately where the rings begin to bend in the direction of nail travel, producing an abrupt interface between compacted and non-compacted wood. Such abrupt borders between compressed and non-compressed early wood cells have been documented previously by compaction experiments (Sandberg, et al. 2021; Inoue, et al. 1990). Quantitatively, the total thickness reduction of an affected annual ring is ≈ 60 % (1104 µm / 1850 µm in Figure 2, where 100 % corresponds to the original, uncompressed thickness). Early-wood thickness is reduced to roughly 50 % (752 µm / 1502 µm), whereas late-wood thickness remains close to its original value. The average deflection (bending) angle of the rings is 35 ° ± 5 °.

Nails with lower density and rigidity, such as beech wood nails with an average density of about 0.7 gcm^{-3} (Niemz, et al. 2025) may bend when driven in, unlike LignoLoc nails with an average density of 1.3 gcm^{-3}. Figure 3 illustrates this behaviour where a beech wood nail was driven into a spruce specimen perpendicular to the grain (T/L-plane), but leaving the specimen deflected by 90° at the R/L-plane.

At the entry side the cross-section of the nail is circular (Fig. 3b), but becomes elliptical (Fig. 3c) at the point of exit. The entry diameter is 5.3 mm, whereas the major and minor axes of the ellipse are 6.4 mm and 3.3 mm, respectively. Consequently, the cross-sectional area decreases by 25%, from 22.06 mm^2 (circular entry) to 16.59 mm^2 (elliptical exit). Assuming an average density of 0.7 gcm^{-3} for beech wood at the entry point, at the exit point it has a calculated density of 0.93 gcm^{-3}, reflecting the compaction of the material during nail penetration.

The origin of the curvature observed in the beech nail is not yet clear. One plausible explanation is that the nail tip becomes asymmetrically loaded as it penetrates the spruce matrix. As illustrated in Figure 3d, the leading edge of the nail is positioned between two late-wood sectors of adjacent annual rings. In softwoods such as spruce, the density contrast between early-wood and late-wood is pronounced: early-wood densities typically range from 0.29 to 0.41 gcm^{-3}, whereas late-wood densities vary between 0.60 and 0.91 gcm^{-3} (Stamm, et al., 2005). The portion of the beech nail that first contacts the wood therefore is surrounded predominantly by spruce late-wood, whose density and mechanical strength are comparable to those of beech. This similarity in material properties can lead to substantial compression of the nail tip, because strength and density are tightly correlated (Savitzky, et al. 1964). The resulting asymmetric compression may generate the bending moment that produces the observed curvature.

Unlike metal, wooden nails and their surrounding wooden matrix can be investigated using computerised tomography (CT). While Korte et al. (2018) presented the first CT image of a wooden nail in spruce, they were unable to demonstrate general aspects. The present work extends the approach by analysing LignoLoc and hornbeam nails of various diameters (2.8 mm, 3.7 mm, 4.7mm and 5.3 mm) and tip-flank angles (15°, 30° and 45°). The tip angle is defined as the angle between the flank of the tip and the longitudinal nail axis; consequently a 15° tip corresponds to a 30° total opening between the two flanks, whereas a 45° tip yields a 90° opening. All four specimens in Figure 4 show a principal crack running in the fibre direction (L), as well as smaller cracks adjacent to it. In CT scans, black voxels represent areas with no detectable X-ray scattering and are interpreted as voids. Dense wood material (e.g., LignoLoc, $\rho \approx 1.3\ gcm^{-3}$) appears as very bright voxels (Fig. 4a, c, d), whereas the less dense hornbeam ($\rho \approx 0.8\ gcm^{-3}$) (Kollmann, 1951) is rendered in a slightly darker grey (Fig. 4b). The reconstructions are based on cubic voxels with an edge length of 4.01 µm. Each voxel stores the average

attenuation coefficient of the material inside it, which is directly related to density. A voxel entirely filled with cell-wall material (e.g., a late-wood tracheid) therefore appears bright, while a voxel that straddles a cell wall and a lumen yields an intermediate grey value. The lumina of tracheids, which contain only air, are rendered black and are indistinguishable from cracks.

In all four panels of figure 4 a dome-shaped zone of increased attenuation is visible in the tangential direction adjacent to the nail. The brightness of these zones matches that of the LignoLoc material, indicating local compaction of the surrounding spruce. In the hornbeam specimen (Fig. 4b) the compacted zones are even brighter, confirming that the outer flanks of the hornbeam nail are also densified by the interaction with the spruce matrix.

As can be seen in Figure 5 (left side), the cracks adjacent to the nails do not have a uniform shape from the head to the tip. In the R/L plane, the CT scan shows more or less pronounced 'fraying', comparable to the upper shot channel in **Error! Reference source not found.** (right side). Where fibres lie against the nail surface, they are also bent and compacted in the longitudinal direction (black arrows). Significant longitudinal compaction is found in the earlywood but is considerably less pronounced in the latewood, which is consistent with the synchrotron radiation micro-computed tomography (SRμCT) findings of Sanabria et al. (2020).

The typical compaction zone accompanying the radially driven nail is found only in the T-direction of the matrix. In the L-direction, cracks of various sizes frequently appear, e.g. in Figure 4. In the longitudinal or grain direction the surrounding wood matrix does not remain in continuous contact with the nail surface. This is in accordance with Korte, et al., 2018, Figure 9. Examining a shot channel in a spruce square timber driven in by a nail a few millimetres below the surface (Fig. 5, reight**Error! Reference source not found.**) reveals that the cracks separate the matrix into individual fibre bundles.

Figure 6 presents a representative CT section of a spruce specimen penetrated radially by a nail. A primary crack runs longitudinally (L-direction) through the wood at the point of nail entry. On either side of the nail, bright-coloured, dome-shaped zones of compaction are visible (outlined in red, square dotted line); these zones fan out along the grain and give the overall pattern a shape reminiscent of a moth's wing (yellow, round spotted outline). Within the dome, individual fibre strands appear slightly brighter than the surrounding strands, indicating a modest density increase. Adjacent to the "wing", two tapering triangular cavities (black) form an X-shaped configuration when the left- and right-hand sides are considered together (black dashed lines). At the interface between the bright fibre strands and the triangular cavities the strands are frayed, which is interpreted as a tensile fracture caused by the nail forcing the fibres to bend and stretch.

The deformation can be explained by the elongation characteristics of spruce. Spruce exhibits a longitudinal strain of approximately 4% ± 2% in the fibre direction (Kollmann, 1951). Fibres that lie directly against the nail surface are subjected to significantly greater local strain. In theory, if a fibre were to lie directly against the surface of the nail semicircle, it would have to be stretched by a factor of $\pi/2$, inevitably leading to breakage. The associated transverse contractions, dictated by Poisson's ratios $\mu LR = 0.376$ (radial) and $\mu LT = 0.42$ (tangential) (Sandberg; et al. 2021), are modest. For an assumed longitudinal strain of 4 % the predicted radial and tangential contractions are 1.5 % and 1.7 %, respectively, values that are too small to generate a noticeable grey-value contrast in the CT images.

In X-ray CT the observed contrast does not scale linearly with material density. Prior to reconstruction the raw projection data were processed with the Phase-Retrieval Operator at ESRF, which enhances phase contrast, especially for structures oriented in the tangential direction. Consequently, the compacted zones appear considerably brighter.

Figure 7 shows a comparison of the same region examined by CT and a reflected-light micrograph of a hornbeam nail driven radially into spruce. The densification of the surrounding wood is far more pronounced in the CT image than in the reflected-light image, highlighting the superior sensitivity of phase-contrast tomography to subtle density variations.

Reflected light microscopy confirms that the 'frayed fibre strands' are cracks within individual fibre strands. Figure 7 shows an enlarged section of a spruce matrix adjacent to the nail, with strain fractures visible at the tips of the individual fibre bundles. These fractures differ in appearance from those found across the tracheids in earlywood, for example, and are more similar to fractures found in the contact areas of two longitudinally connected tracheids in latewood (Sandberg, et al., 2021). Cracks running across the tracheids would be perpendicular to the direction of the fibres and would have a frayed appearance. As density significantly affects tensile strength, it is clear that tensile cracks do not occur within the compacted, dome-shaped regions, but rather next to them where compaction does not occur.

The recognition that cracks around nails are caused by the splitting of the nail by the tip and by tensile failure has led to the development of a new nail tip design.
The hypothesis was that cracks deliberately created by the tip geometry would envelop the nail shaft more uniformly than cracks that occur randomly. Rather than having a conical or pyramidal tip, the new design has four sharp cutting edges. The tip can be imagined as that of a Phillips screwdriver with sharpened flanks (see Fig. 8). During driving, these sharp edges cut the fibres, thereby preventing spontaneous tearing under tension. This significantly reduces the tensile stresses around the nail, thereby minimising the risk of cracking.
EUROCODE 5 (DIN, 2010) requires that nails be spaced at least seven nail diameters (7d) perpendicular to the grain in timber with a density > 0.42 gcm^{-3}, and at least five diameters (5d) in timber with a density < 0.42 gcm^{-3}, in order to minimise strength losses due to cracking. In order to test the effectiveness of the new 'Phillips-tip' with steel and LignoLoc nails (both d = 4.7 mm), they were driven into tongue-and-groove larch (*Larix decidua*) boards to fix them to underlying solid structural timber. No cracks were observed when the nails were spaced at the prescribed 7d (≈ 33mm). Remarkably, cracks did not appear until the spacing was reduced to 2 d (≈ 9.4 mm). This reduction in the required nail-to-edge distance has significant commercial relevance. For a conventional 5 mm nail, the EUROCODE 5 edge distance of 3.5 cm (7 d) dictates a minimum width of 7 cm for square timber sub-frames. However, if any inaccuracies occur when driving the nails, the required beam size of 8 cm or more, which is standard in Germany, will quickly be reached. In Scandinavia, however, substructures with timber joists as narrow as 27 mm are used (Metsä). The 'Phillips-tip' may enable reliable fastening of such slender members, extending the range of applicable timber dimensions.
When a LignoLoc nail with a 'Phillips-tip' radially driven into spruce wood, is examined by CT scan, the characteristic compacted caps, the ‘moth wings’ and the X-shaped cracks are also visible (Fig. 9). The CT images in Figure 9 differ from Figure 6 in that way, that they also show more compacted matrix material along the grain of the nail. This longitudinal compaction is especially pronounced in the upper left figure of Figure 9 (1-0828). Figure 9 shows the LignoLoc nail in successive cross-sectional planes at 100-voxel increments of 3800 µm, starting at the top left with the entry point into the spruce matrix and extending to the cross-shaped nail tip at the bottom right (1-1328). The X-shaped cracks, created by the nail's sharp and X-shaped edges are clearly visible in the matrix.
The observations demonstrate that cracking around nails is often either overlooked or significantly underestimated in conventional design calculations. Zhang et al. (2025) determined the specific nail withdrawal capacity by relating it to the nominal contact area between the nail and wood matrix.

3.2 Chemical characterization

When a nail is driven into a wooden matrix, frictional heat is generated at the nail's surface and within the matrix. Korte et al. (2026) found that the friction heat on the nail surface was approximately 200 °C ± 15 °C. Driving speeds are in the range from about 30 to 50 ms^{-1} and insertion times range from 1 to 3 ms. This is more than a thousand times faster than friction wood welding, which takes between 2 s (Gfeller, et al., 2004) to 18 s to form a welded joint (Stamm, et al., 2005; Stamm, et al., 2006). Wood welding processes differ greatly in terms of maximum temperatures. Linear oscillating friction with beech wood at 100 Hz reached approximately 200 °C (Gfeller, et al., 2004) whereas circular oscillating friction welding with spruce resulted in temperatures of up to 440 – 450 °C in the contact zone of the friction partners (Stamm, et al., 2005; Stamm, et al., 2006). In both cases, a layer with a molten lignin polymer matrix and a wood cell/fibre entanglement network is formed. Crosslinking chemical reactions have also been observed (Gfeller, et al., 2004; Gfeller, et al., 2003). During wood friction welding, however, low-molecular-weight degradation products can be produced and as a result, joints produced by wood friction welding are often sensitive to water (Pena, et al., 2016).
This raises the question of whether comparable welding processes take place under the milder conditions of nail insertion, which degradation products occur, or whether other mechanisms are at work, such as the squeezing out of lignin onto the contact surface (Wang, et al., 2025), polymer degradation (Stamm, et al., 2006) or carbonisation, creating typical components such as tar pitch and bright coal (Suthoff, et al. 1996), are at work.
In order to investigate the effect of thermal stress to chemical constituents of the material in the contact zone between the nail and the matrix, nails (LignoLoc, beech and hornbeam) were shot into spruce square timber. The layers of the contact zone were collected by the method described above and then extracted for further analyses. These extracts were analysed rather than material scraped from these layers, since thermal stress caused by friction alters a small proportion of the wood's most important polymeric constituents. These constituents then become soluble in a mixture of acetone and water.

3.2.1 SEC

Nuclear magnetic resonance (NMR) spectroscopy and high-performance liquid chromatography (HPLC) methods were unable to identify substances such as hexoses and pentoses in the form of oligomers, monomers, and/or their thermal degradation products (e.g. levoglucosan) in the extracts obtained from the interface (Harima 2021). Such compounds are present in wood friction-welded joints (Pena, et al., 2016;). This difference might be attributed to the short reaction time during the injection of nails which is not sufficient for initiating complex sequences of degradation reactions.

Size exclusion chromatography (SEC) revealed a shift of UV active compounds to slightly higher molecular weights in the adhering fibres (Fig. 10, WN-sample Ø 4.9 mm) compared to thermally unaffected matrix material (Fig. 10, spruce reference (a, b, c)) and the LignoLoc nail reference (WN reference).

In the high molecular weight (Mw) range (> 8.000 $gmol^{-1}$), the molecular weights of the WN samples (1490–1900 $gmol^{-1}$) were higher than those of the spruce reference (760–1200 $gmol^{-1}$) and wood nail reference samples (1,130 $gmol^{-1}$). This suggests that cross-linking of lignin may have occurred. The mean molecular weight of the WN sample Ø 4.9 with 1,900 $gmol^{-1}$ is slightly higher than that of the WN samples Ø 4.8 with 1,890 $gmol^{-1}$ but significantly higher than the molecular weights of WN sample Ø 4.7 with 1,490 $gmol^{-1}$and the wood nail reference at 1,130 $gmol^{-1}$.

3.2.2 Py-GC/MS

To investigate chemical changes within the higher molecular weight range, the extracts of WN samples and various reference materials (spruce and wooden nails, both with and without phenolic resin) were analysed by Py-GC/MS. To detect any changes in lignin, the HGS building blocks of the lignins were examined: the p-hydroxyphenyl (H), guajacyl (G) and syringyl (S) elements. Spruce lignin consists of G elements with only small proportions of HS building blocks, whereas beech lignin consists of GS elements and contains only small proportions of H building blocks (Windeisen, et al., 2012). LignoLoc nails contain two types of H building blocks: one from the beech wood veneers and the other from the phenolic resin. The GC/MS data were analysed to determine the HGS lignins and carbohydrate building blocks. Following Romagnoli et al. (2018), thermal stress has an effect on the chain length of lignin pyrolysis products. For this reason, the monomeric guajacyl (G) lignin pyrolysis products were investigated to determine the impact of thermal stress resulting from nail insertion on the lignin in the contact area between the WN and the spruce wood. Within this group, various compounds can be distinguished based on the length of their side chains (Fig. 11).

Broadly speaking, these can be divided into two types of G-lignin: those with short side chains (G-SC), which have up to two carbon atoms attached to the aromatic ring; and those with long side chains (G-LC), which have more than two aliphatic carbon atoms in the side chain.

When lignin is subjected to thermal stress, such as that generated by driving wooden nails into wood, the proportion of G-SC in the pyrolysis products increases, while the proportion of G-LC decreases (Romagnoli et al., 2018). Consequently, the SC/LC ratio of G-lignin pyrolysis products rises. The peak areas of the lignin pyrolysis products in the chromatogram were therefore determined and summed according to their chain length.

Analyses with Py-GC/MS show that the various spruce reference samples are very similar, with an SC/LC ratio of 1.3–1.4. In contrast, fibres scraped from LignoLoc nails have a significantly higher SC/LC ratio of 2.4–3.2 (Tab. 1).

For the material of fibre fraction of 5.1 mm (Tab. 1) and an SC/LC ratio of 2.4, it can be assumed that this fibre fraction consists solely of adhering spruce material, given the nominal nail diameter of 4.7 mm. The ratio of fibre fraction of 4.9 mm is higher than that of the adjacent layer. The SC/LC ratio is significantly higher than that of the spruce reference. Spruce material is also to be expected, at least in part, for the layers further inwards (4.8 mm and 4.7 mm). The decreasing SC/LC values (2.4) suggest a lower thermal load here. If the adhering spruce material were mixed with the nail material, the values would not decrease, but increase, as LignoLoc nails have a ratio between 3.3 and 3.6. The highest layer value of 3.2 is found in the fraction produced by the 4.6 mm diameter hole. Since the LignoLoc nails have a nominal diameter of 4.7 mm, it can be assumed that these samples largely consist of LignoLoc material.

Similar results were obtained from the analysis of the deposits on hornbeam nails, although the interface SC/LC ratio was only 1.7 and the hornbeam nails themselves had a ratio of 2.4 (Tab. 1). These results suggest that thermal alteration of the lignin occurred in the adhering layers during the driving-in process. While the lignin might be

more crosslinked by the thermal effect the treatment intensity is not strong enough to induce intense thermal degradation reaction which might form unfavourable low molar mass degradation products.

3.2.3 UMSP

Based on the scanning UV-microspectrophotometry (UMSP) analyses conducted by Korte et al. (2018), samples containing beechwood nails were analysed. alongside those containing LignoLoc to detect the modification of lignin and phenolic extractives on a cellular level.

Figure 12 shows an ultramicrotome section (thickness of 1µm) of a LignoLoc nail and the adjacent spruce matrix, as well as the interface between the two materials. Cross sections of beech cells are visible at the LignoLoc, e.g. in field 1 of Figure 12. On the spruce side, tracheids can be seen in the radial direction with longitudinal elongation, for example in field 3. Fields 5 and 6 represent the interface region between the two materials. There is no distinguishable morphological layer in Figure 13, e.g. molten cell material with entangled detached wood cells (Gfeller, et al. 2004), detectable.

Fig. 13 presents UV microspectrophotometric area scans of the regions highlighted in yellow in Figure 12. The UV absorbance values, comprising 4,096 grey-scale levels, are displayed using 14 false colours, as indicated by the colour scale on the left side of each image. The colour coding represents the UV absorbance of lignin and phenolic extractives at a wavelength of 278 nm. The two upper scans show cross-sections of beech fibres in LignoLoc. Most secondary cell walls exhibit a reddish colour, which corresponds to the typical UV absorbance of normally lignified S2 cell wall layers. The black deposits within the lumina of fibres and parenchyma cells are indicative of highly condensed phenolic compounds. These may have been formed during thermal modification in the compreg process, or may be the result of phenol resin.

The two central scans show spruce tracheids in radial longitudinal view. The elongated white areas correspond to the tracheid lumina.

The two lower scans (fields 5 and 6) represent the interfacial region between the LignoLoc nail and the surrounding spruce wood. The large white area in field 5 is a preparation-induced crack that is also visible in Figure 12. In field 6, the compressed spruce tracheids (upper part) are in direct contact with the beech fibres of LignoLoc (lower part of the image), and no distinct interfacial layer separating the two materials can be identified.

High-resolution UV scans reveal distinct regions of very high UV absorbance ($A > 1.0$; black areas) at the interface between the highly compressed wood tissue and the LignoLoc nail. These high absorbance values indicate the formation of highly condensed phenolic reaction products resulting from thermal modification and compression-induced merging of the lignified cell wall matrix and phenolic extractives.

Figure 14 shows an ultramicrotome section of a beech wood nail with an adjacent spruce wood matrix, along with the marked rectangles that were analysed using UV absorption spectrometry. Figure 15 shows the corresponding ultraviolet (UV) scans of the yellow-marked areas.

The two upper images of Figure 15 show beech wood cells in cross-section that have not been densified or filled. The two middle images are comparable to those in Figure 12. The two lower images, however, are difficult to interpret without the context of Figure 13. Additionally, no layer of differently structured material can be found between the nail and the matrix.

The absence of an interface layer sets this process apart from traditional wood welding methods, where layers are identified using light microscopy (Stamm et al., 2005), scanning electron microscopy (Gfeller et al., 2004; Leban et al., 2005) or X-ray microdensitometry (Leban et al., 2005). In X-ray microdensitometry studies, layer thicknesses were reported as 0.6 mm for beech and 1.8 mm for spruce. The density increases from the spruce (approx. 500 g cm^{-3}) and beech (approx. 800 g cm^{-3}) surrounding matrix to over 1000 g cm^{-3} in the layer of molten material. If comparable molten layers existed between the beech wooden nail and the spruce matrix, they would be discernible in the UMSP, which has a resolution of 0.25 µm² (Korte et al., 2018).

The two upper images in Figure 15 show the characteristic UV absorbance pattern of uncompressed, unmodified beech wood cells in cross-section. The blue colours correspond to the S2 cell wall layers, which exhibit typical UV absorbance values between 0.15 and 0.20. The compound middle lamella and cell corners of adjacent fibres are characterised by higher UV absorbance values ranging from 0.30 to 0.40 and are displayed in red and violet. This distribution is characteristic of normal lignin distribution in beech wood tissue.

The two central images in Figure 15 are comparable to those shown in Figure 13 and show the UV absorbance distribution of the individual cell wall layers in longitudinal section. Regions with very high UV absorbance values ($A > 1.0$; signal overflow) are visible within the fibre lumina and are attributed to highly condensed phenolic

compounds formed during thermal modification. These compounds are particularly prevalent in the highly compressed and densified tissue at the interface (friction zone) between the wood tissue and the nails. In these regions, the wood tissue is compressed to such that the individual cell wall layers can no longer be clearly distinguished, as can be seen in the lower images of Figure 15.
UV absorption spectra were measured for selected cell structures (Fig. 16), such as the cell corner (CC), the compound middle lamella (CML) and the secondary wall 2 (S2) in the range from 240 nm to 500 nm.
The UV absorbance at 280 nm was consistently higher at the LignoLoc/spruce interface than at the beech wood nail/spruce interface. As the wood matrix of the LignoLoc nails is also made of beech wood, this difference is attributed to the additional contribution of the phenolic resin to the UV absorbance.
In addition to the UV area scans, point spectra were recorded with a spot size of 1 µm² and a wavelength range of 240–500 nm. Figure 16 shows representative spectra of the lignified S2 cell wall layer and the compound middle lamella (CML) of undamaged spruce tracheids. Both spectra exhibit the characteristic absorbance pattern of softwood lignin, with a distinct maximum at around 280 nm and a local minimum near 250 nm (Koch et al., 2013). The absorbance maximum at 280 nm is characteristic of guaiacyl-rich lignin and typically ranges from $A_{280} = 0.35$ in the S_2 layer to $A_{280} = 0.80$ in the CML.
Representative UV absorbance spectra of the S2 layer and the CML in compressed and densified cell walls adjacent to the wood-nail interface are also presented. Compared with unaffected spruce tissue, both cell wall regions exhibit a pronounced increase in UV absorbance, with A_{280} values ranging from approximately 0.9 to 1.8. This increase is more pronounced at the LignoLoc/spruce interface than at the beech wood nail/spruce interface, indicating an additional contribution from the phenolic resin incorporated into the LignoLoc nail.
This marked increase in UV absorbance is consistent with thermally induced modifications to the lignin structure. According to Nimz (1973), increasing temperatures promote the formation of conjugated double-bond systems within lignin. This results in enhanced π–π^* electronic transitions and consequently increased UV absorbance. These chemical modifications can be clearly resolved at the cellular level by UV microspectrophotometry.

4 Conclusions

- There is a zone of compaction in the matrix that runs parallel to the nail and transitions abruptly into uncompacted material. There is no zone of decreasing density.
- From the impact pattern of radially driven nails, it is possible to analyse the displacement and compaction processes during impact. This quasi-frozen state can be observed in the matrix sectioned in the T/R plane.
- Matrix changes such as compaction and/or the formation of holes and cracks are direction-dependent (R, T and L directions).
- - A driven nail is rarely completely encased or enveloped by matrix material. This means that the assumptions in standards (e.g. DIN 1382, DIN Deutsches Institut für Normung e.V., 2016) and literature (e.g. Zhang, et al., 2025) are incorrect.
- Matrix material bends in the driving direction within a certain angular range.
- The compaction zone in the matrix material is proportional to the nail diameter.
- Solid wood nails made of beech or hornbeam are also compacted, but only to a minor extent compared to the spruce matrix.
- Crack formation consists of transverse splitting and tensile cracks running parallel to the grain.
- - CT scans in this research are mathematically processed to highlight differences in density. This makes it easier to identify compacted 'tensile fibres'.
- - With round-tipped nails, the wood matrix is compacted in the tangential direction while cracks form parallel to the grain. Due to these cracks, the surrounding wood matrix does not make contact with the nail in all positions. However, a new nail tip geometry featuring sharp cutting edges significantly reduces the splitting effect, resulting in more matrix material surrounding the nail.
- Chemical analyses indicate
- - no low-molar-mass degradation products in the interface layer
- Crosslinking of lignin in wood occurs in the interface layer.
- In solid wood nails, thermally induced changes in lignin can be detected within the nail material itself using USMP.
- There is no boundary layer consisting of molten material and detached fibres between the nail and the matrix.
- The nail-matrix transition zone contains no degraded polysaccharides.

- In the boundary layer between the nail and the spruce wood matrix, a change in the spruce lignin was detected. This is manifested by an increase in molecular weight, a change in the side groups of the lignin building blocks and an increase in UV absorption.

5 Literature

Bergsagel, D., Heisel, F., Owen, J., Rodencall, M. (2025). Engineered wood products for circular construction - a multi-factor evaluation of lamination methods. Materials sustainability, 3(24), p. 25.

Bruzzone, G., Moya, L., Vicente, W. M., da Silva Guedes, R., Quagliotti, S., Passarella, D. (2026). Flexural performance of adhesive-free and metal-free laminated timber panels: Experimental, analytical and numerical analysis. Journal of Building Engineering, p. 116786. doi:10.1016/j.jobe.2026.116786

Bucklin, O., Di Bari, R., Amtsberg, F., Menges, A. (2023). Environmental impact of a mono-material timber building envelope with enhanced energy performance. Sustainability, 15(556), p. 20. doi:https://doi.org/10.3390/su15010556

Crovella, P., Olaosebikan, O. (2025). Performance of Nail-Laminated Timber assembled with Wood-Based Fasteners. World Conference on Timber Engineering (WCTE 2025) (pp. 4145-4152). Brisbaine, Australia: World Conference on Timber Engineering. doi:https://doi.org/10.52202/080513-0509

DIN Deutsches Institut für Normung e.V. (2016). DIN EN 1382 Timber structures - Test methods - Withdrawal capacity of timber fasteners; German version EN 1382:2016. Berlin: Beuth Verlag GmbH.

DIN, N. B. (2010). Eurocode 5: design of timber structures - Part 1-1: General - Common rules and rules for buildings; german version EN 1995 -1-1:2004 + AC.20066 + A1:2008. Berlin: Beuth Verlag GmbH.

Fan, W., Zhu, X., Hu, X., Liu, H. (2025). Effect of wet–dry cycles on the shear behavior of compressed wood nails compared to steel nails. Forests, 16(940), p. 10. doi:https://doi.org/10.3390/f16060940

Gerber, L., Eliasson, M., Trygg, J., Moritz, T., Sundberg, B. (2012). Multivariate curve resolution provides a high-throughput data processing pipeline for pyrolysis-gas chromatography/mass spectrometry. J Anal Appl Pyrol, 94, pp. 95-100.

Gfeller, B., Pizzi, A., Zanetti, M., Properzi, M., Pichelin, F., Lehmann, M., Delmotte, L. (2004). Solid wood joints by in situ welding of structural wood constituents. Holzforschung, 58.

Gfeller, B., Properzi, M., Zanetti, M., Pizzi, A., Pichelin, F., Lehmann, M., Delmotte, L. (2004). Wood Bonding by Mechanically-Induced in Situ Welding of Polymeric Structural Wood Constituents. Journal of applied Polymer Science(92), pp. 243-251.

Gfeller, B., Zanetti, M., Properzi, M., Pizzi, A., Pichelin, F., Lehmann, M., Delmotte, L. (2003). Wood bonding by vibrational welding. Journal of Adhesion Science and Technology, 17, pp. 1573-1589.

Giordano, L. (2022). Developing dowel-laminated timber panels from short salvaged timber elements. (Master Thesis), 77. Politecnico di Torino.

Han, L., Kutnar, A., Sandak, J., Sustersic, I., Sandberg, D. (2023). Adhesive-and Metal-Free Assembly Techniques for Prefabricated Multi-Layer Engineerd Wood Products - A Review on Wooden Connectors. Forests, 14(311).

Harima, A. (2021). Chemische Veränderungen an der Grenzfläche von Holz und Holnägeln (Chemical changes at the interface area of wood and wooden nails). Hamburg: University of Hamburg.

Hasan, H., Reddy, A., TsayJacobs, A. (2019). Robotic Fabrication of Nail Laminated Timber. p. 7.

Heisel, F., Bergsagel, D. (2025). Structural reclaimed wood - reuse, re-reuse, and repurposing. In R. Hvejsel, & F. Hvejsel, Structures in Architecture (p. 8). USA: CRC Press. doi:10.1201/9781003658641-3

Inoue, M., Norimoto, M., Otsuka, Y., Yamada, T. (1990). Surface compression of coniferous wood lumber I. A new technique to compress the surface layer. Mokuzai Gakkaishi, 36, pp. 224-235.

Khan, I., Subhani, M., Ghabraie, K., Ashraf, M. (2025). Mechanical performance and design challenges of wooden fasteners - a critical analysis of evaluation methods and standards. European Journal of Wood and Wood Products, 83(143), p. 30.

Koch, G., Schmitt, U. (2013). Topochemical and Electron Microscopic Ansalyses on the Lignification of Individual Cell Wall Layers During Wood Formation and secondary Changes. In G. Koch, U. Schmitt, & J. Fromm (Ed.), Cellular Aspects of Wood Formation, Plant Cell monographs 20. Berlin, Heidelberg: Springer-Verlag.

Kollmann, F. (1951). Technologie des Holzes und der Holzwerkstoffe (Technology of wood and wooden products) (2. ed., Vol. 1). Berlin, Göttingen, Heidelberg: Springer Verlag.

Korte, H., Fey, A., Diestel, S. (2026). Nail gun insertion of wooden nails into wood. Exploratory Materials Science Research, 1, pp. 29-41.

Korte, H., Koch, G., Krause, K. C., Koddenberg, T., Siemers, S. (2018). Wood nails to fix softwoods: characterization of structural deformation and lignin modification. European Journal of Wood and Wood Products, pp. 979–988.

Leban, J. M., Pizii, A., Properzi, M., Pichelin, F., Gelhaye, P., Rose, C. (2005). Wood welding: A challenging alternative to conventional wood gluing. Scandinavian Journal of Forest Research, 20, pp. 534-538.

Leban, J. M., Pizzi, A., Wieland, S., Zanetti, M., Properzi, M., Pichelin, F. (2004). X-ray microdensitometry analysis of vibrationa-welded wood. J. Adhesion Sci. Technol., 18(6), pp. 673-685.

Metsä. (n.d.). Kerto LVL. Retrieved 04 27, 2026, from Studs for wall structures: https://www.metsagroup.com/metsawood/products-and-services/products/kerto-lvl/t-stud/

Neagu, C. R., Gamstedt, K. E., Bardage, S. L., Lindström, M. (2006). Ultrastructural features affecting mechanical properties of wood fibres. Wood Material Science and Engineering, 1(3-4), pp. 146-170.

Niemz, P., Caduff, D. (2008). Untersuchungen zur Bestimmung der Poissonschen Konstanten an Fichtenholz (Invetigation into the determination of Poisson's ratios in spruce wood). Holz Roh. Werkst.(66), pp. 1-4. doi:10.1007/s001707-007-0188-2

Niemz, P., Teischinger, A., Sandberg, D. (2023). Handbook of Wood Science and Technology. Cham, Switzerland: Springer. doi:https://doi.org/10.1007/978-3-030-81315-4

Niemz, P., Teischinger, A., Sandberg, D. (2025). Wood Material and Processing Data - The most relevant data, tables and figures. Cham, Switzerland: Springer. doi:https://doi.org/10.1007/978-3-031-38329-8

Nimz, H. (1973). Chemistry of potential chromophoric groups in beech lignin. Tappi, 56, pp. 124-126.

Pena, M., Deutschle, A., Saake, B., Pizzi, A., Pichelin, F. (2016). Study of the solubility and composition of welded wood material at progressive welding times. Eur. J. Wood Prod., pp. 191-201.

Pizzi, A., Leban, J.-M., Kanazawa, F., Properzi, M., Pichlin, F. (2004). Wood dowel bonding by high-speed rotational welding. Journal of Adhesion Science and Technology, 18(11), pp. 1263-1278.

Romangnoli, M., Vinciguerra, V., Silvestri, A. (2018). Heat treatment effect of lignin and carbohydrates in Corsican Pine earlywood and latewood studied by Py-GC-MS technique. Journal of Wood Chemistry and Technology, pp. 57-70.

Ruan, G., Filz, G. H., Fink, G. (2022). Shear capacity of timber-to-timber connections using wooden nails. WOOD MATERIAL SCIENCE & ENGINEERING, 10(1), pp. 20-29. doi:https://doi.org/10.1080/17480272.2021.1964595

Sanabria, S. J., Baensch, F., Zauner, M., Niemz, P. (2020). In-situ quantification of microscopic contributions of individual cells to macroscopic wood deformation with synchrotron computed tomography. Scientific Reports, 1, p. 16.

Sandberg, D., Kutnar, A., Karlsson, O., Jones, D. (2021). Wood Modification technologies - Principles, Sustainability and the Need for Innovation. Boca Raton, London, New York: CRC Press.

Savitzky, A., Golay, M. J. (1964). Smoothing and Differentiation of Data by Simplified Least Squares Procedures. Analytical Chemistry, 36(8), pp. 1627–1639. doi:https://doi.org/10.1021/ac60214a047

Schütt, F., Haas, N. P., Dehne, L., Koch, G., Janzon, R., Saake, B. (2013). Steam pretreatment for enzymatic hydrolysis of poplar wood: Comparison of optimal conditions with and without SO2 impregnation. Holzforschung,(1), pp. 9–17. doi:https://doi.org/10.1515/hf-2012-0076

Stamm, B., Natterer, J., Navi, P. (2005). Joining wood by friction welding. Holz als Roh- und Werkstoff, 63, pp. 313-320. doi:10.1007/s00107-005-0007-6

Stamm, B., Windeisen, E., Natterer, J., Wegener, G. (2006). Chemical investigations on the thermal behaviour of wood during friction welding. Wood Science and Technology, 40, pp. 615-627.

Suthoff, B., Schaaf, A., Hentschel, H., Franz, U. (1996). Deutschland Patent No. 19620273C2.

Wang, S., Lin, J., Jin, B., Kong, F., Ma, P., Wang, F., Que, Z. (2025). Group Effect on In-Plane Shear Performance in Wooden Nail Connections. Buildings, 15(1189), p. 16. doi:https://doi.org/10.3390/buildings15071189

Wang, S., Lin, J., Wang, F., Wang, Y., Kong, F., Ma, P. (2025). Mechanical behavior and theoretical modeling of wooden nails under various stress conditions. Construction and Building Materials, 458, p. 139624.

Wang, S., Wang, F., Ma, P., Kong, F., Beck, C., Siemers, S., Que, Z. (2025). Eco-friendly wooden nails: Bonding mechanisms and withdrawal resistance in sustainable timber connections. journl of Cleaner Production(486), p. 144606.

Windeisen, E., Wegener, G. (2012). 10.15 - Lignin as Building Unit for Polymers. In M. K., & M. M., Polymer science: A comprehensive reference (Vols. 1-10 [New ed.], pp. 255-265). Elsevier Science. doi: https://doi.org/10.1016/B978-0-444-53349-4.00263-6

Zhang, S., Li, X., Chen, X., Huang, R., Shen, H., Yang, C., Zhang, Y., Yang, S., Qiu, J., Yang, Y., Liu, L. (2026). Cell-Wall-Engineered Wood Enabling Metal-and-Adhesive-Free Cross-Laminated Timber. Research, 9, p. 12. doi:https://doi.org/10.34133/research.1355

Zhang, Y., Ottenhaus, L.-M., Singh, T., Yermán, L. (2025). The importance of wood relaxation when studying nail withdrawal capacity. Case Studies in Construction Materials, 23, p. e05421.

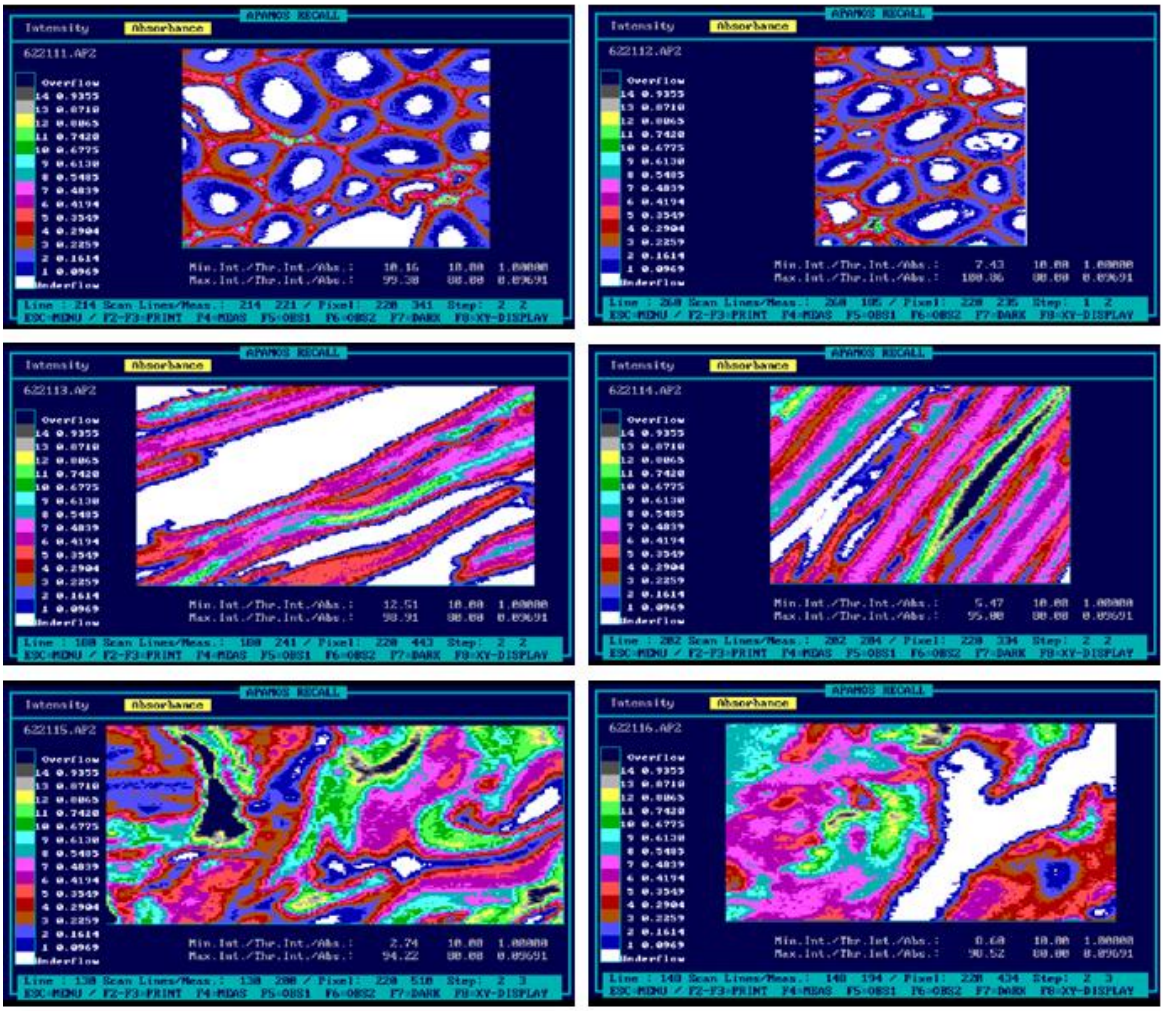


Fig. 15 UV microspectrophotometry area scans of selected parts marked in Fig. 19. Fields 1 and 2 = beechwood nail, fields 3 and 4 = spruce matrix, fields 5 and 6 = the interface between nail and matrix.

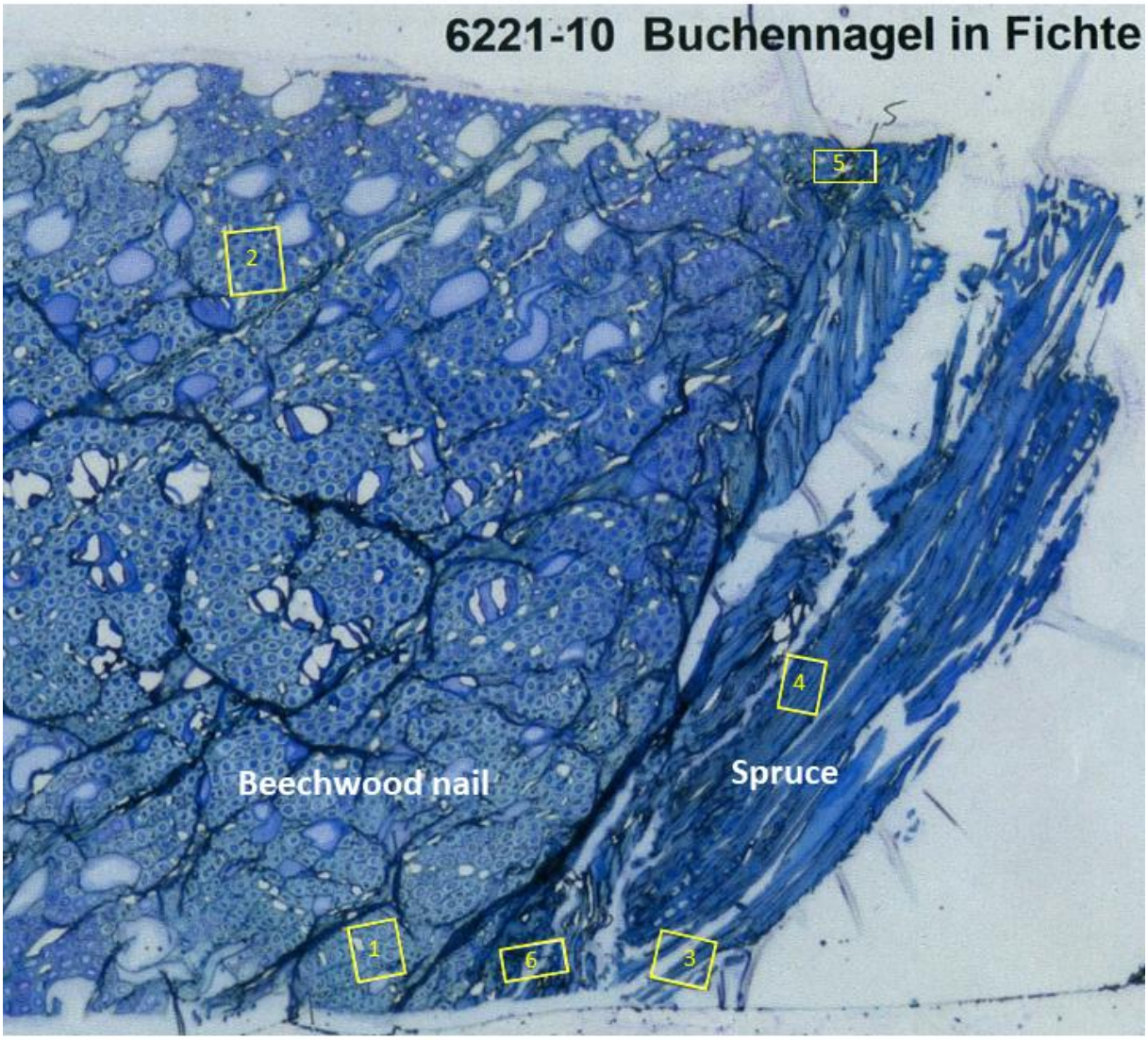


Fig. 14 Ultramicrotome section of a beech wood nail and adjacent spruce wood matrix

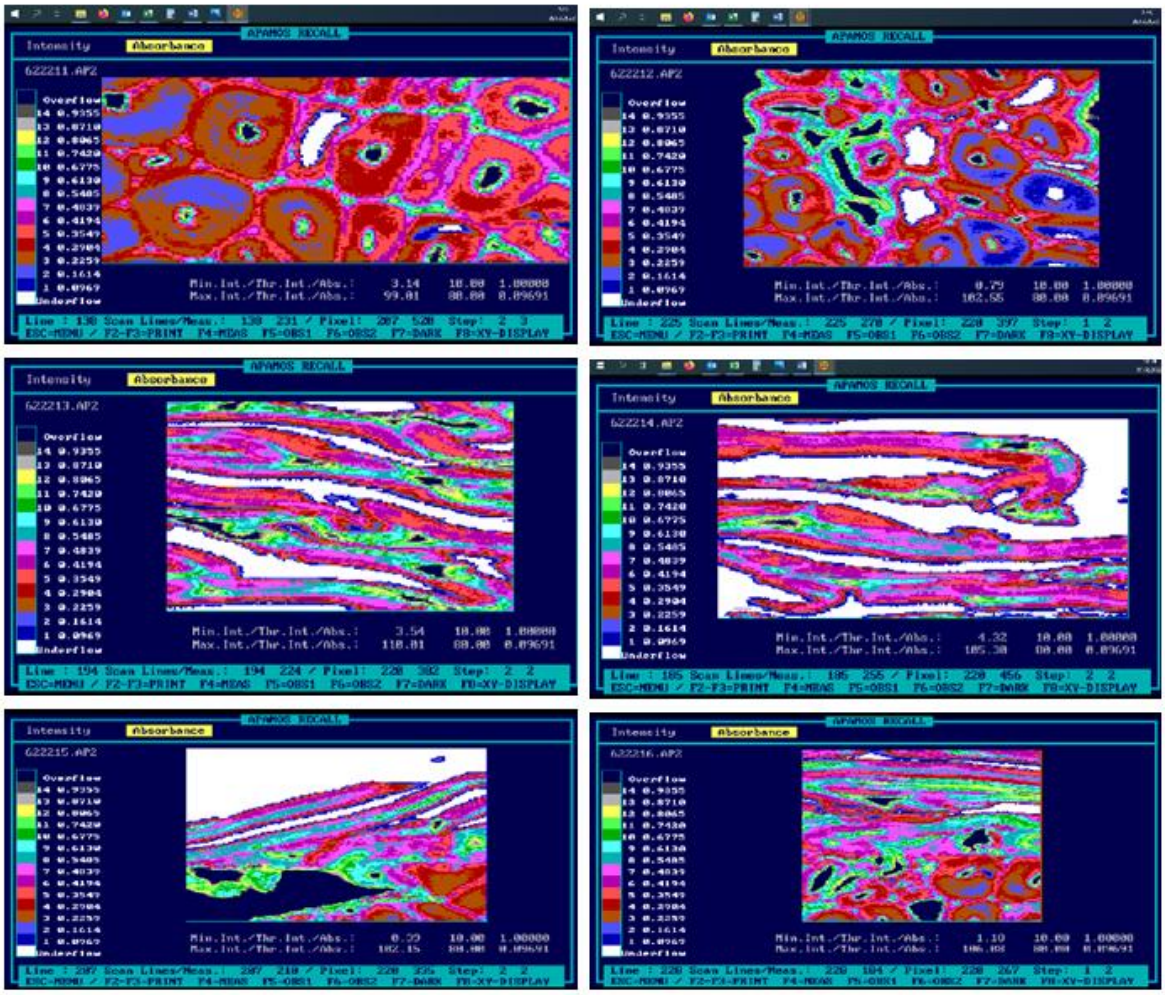


Fig. 13 UV microspectrophotometry area scans of selected parts marked in Fig. 17. Fields 1 and 2 = Lignoloc, fields 3 and 4 = Spruce matrix, fields 5 and 6 = the interface between nail and matrix.

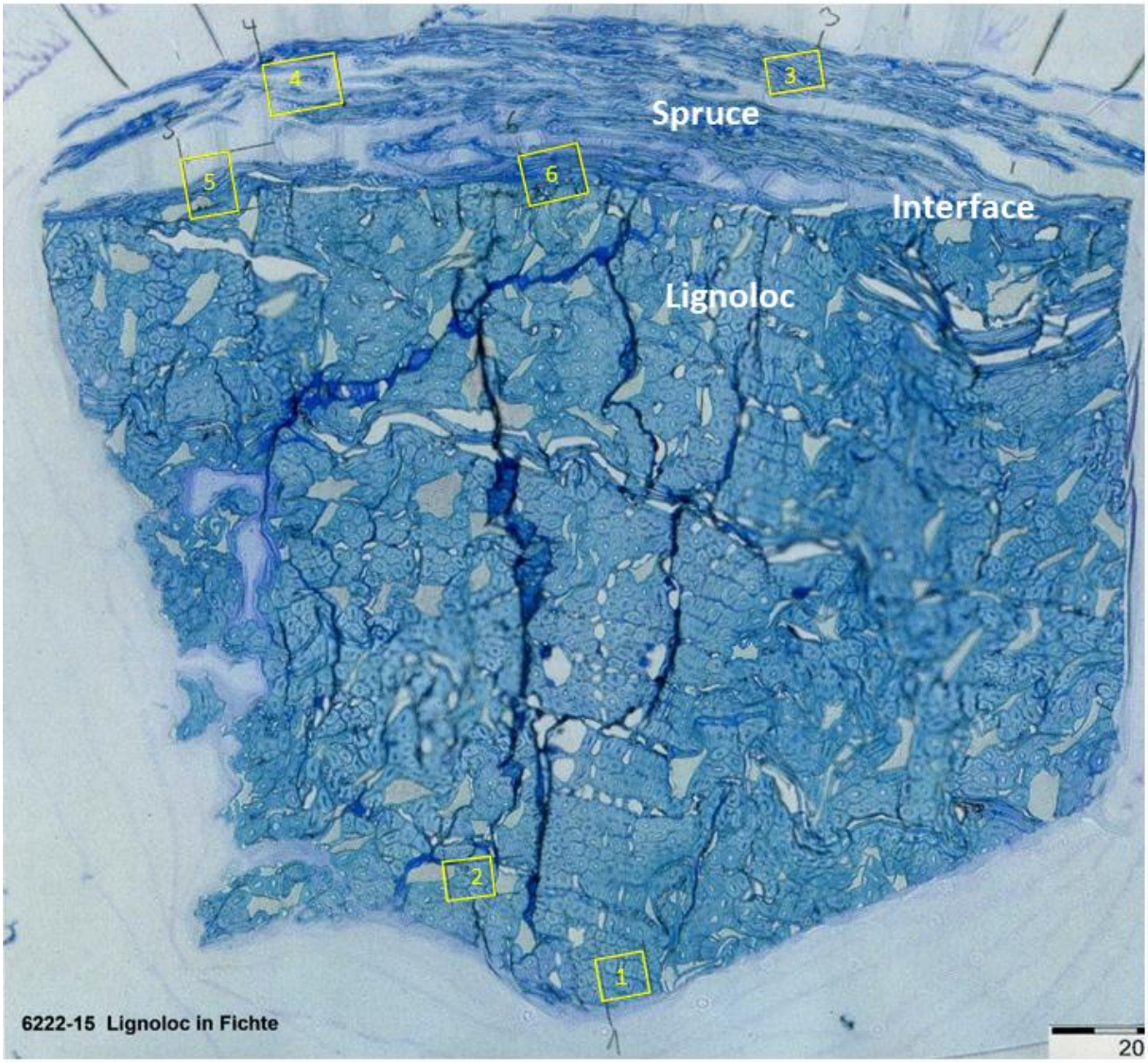


Fig. 12 Ultramicrotome section (thickness of 1µm) of a Lignoloc nail and adjacent spruce wood matrix.

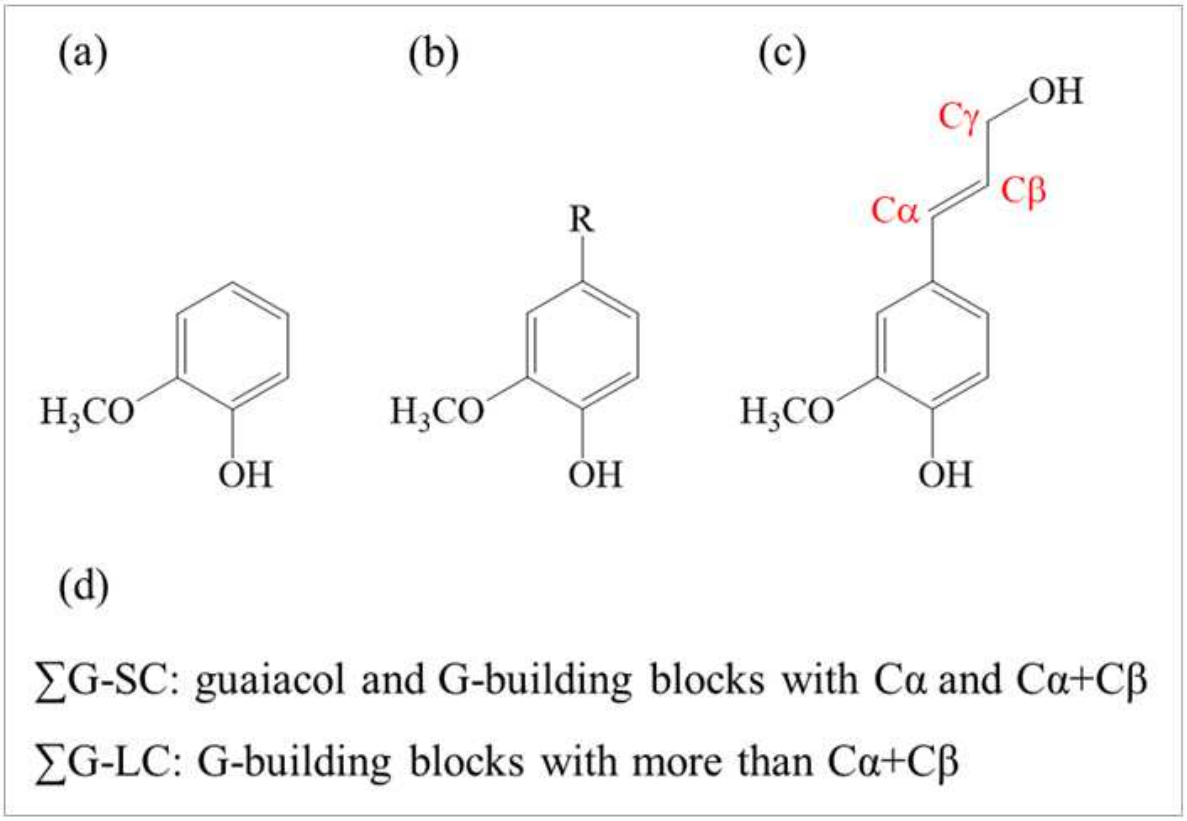


Fig. 11 Guaiacol (a), the guaiacyl building block (b), and coniferyl alcohol (c) are examples of the classification of guajacyl (G) lignins according to the length of their side chains at the Cα, Cβ, and Cγ positions. (d) shows the classification of G-lignins according to side-chain length, where ∑G-SC represents the sum of G-building blocks with short side chains, and ∑G-SC those with long side chains.

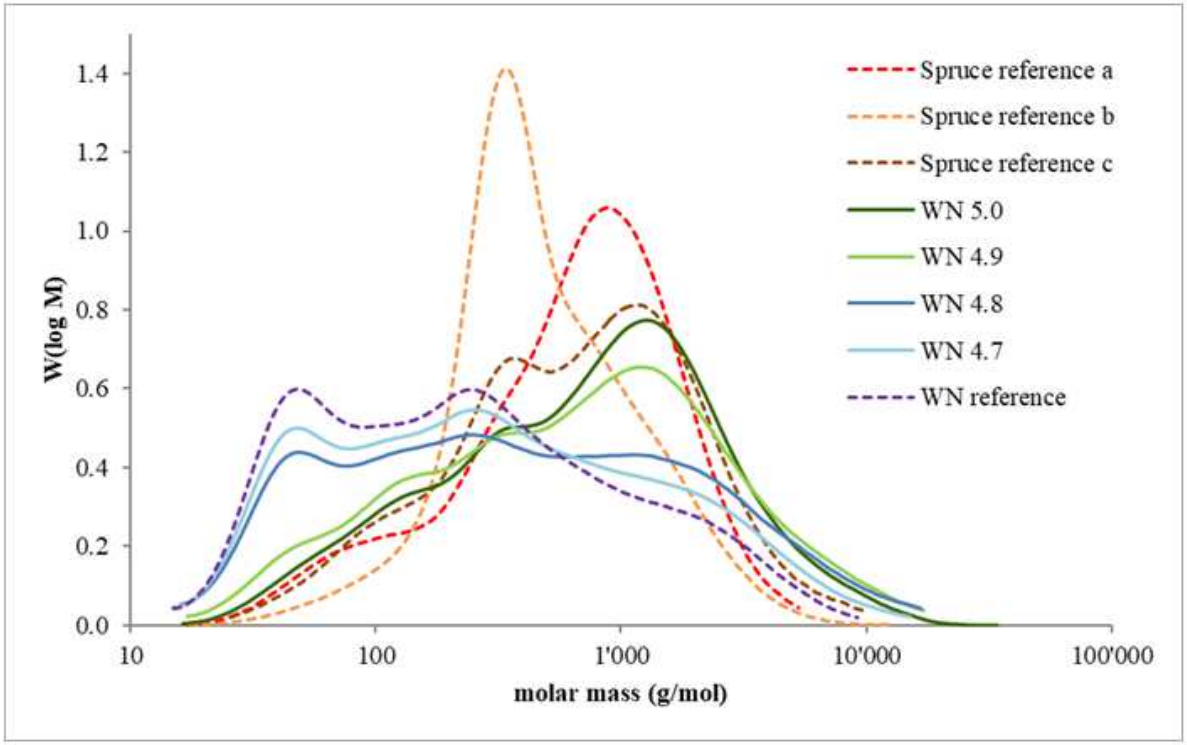


Fig. 10 Molecular weight distribution of acetone-water extracts from adhered wood fibres (WN 4.7, 4.8, 4.9 and 5.0), spruce blank values (spruce references a, b and c) and a Lignoloc nail (WN reference), as determined by SEC

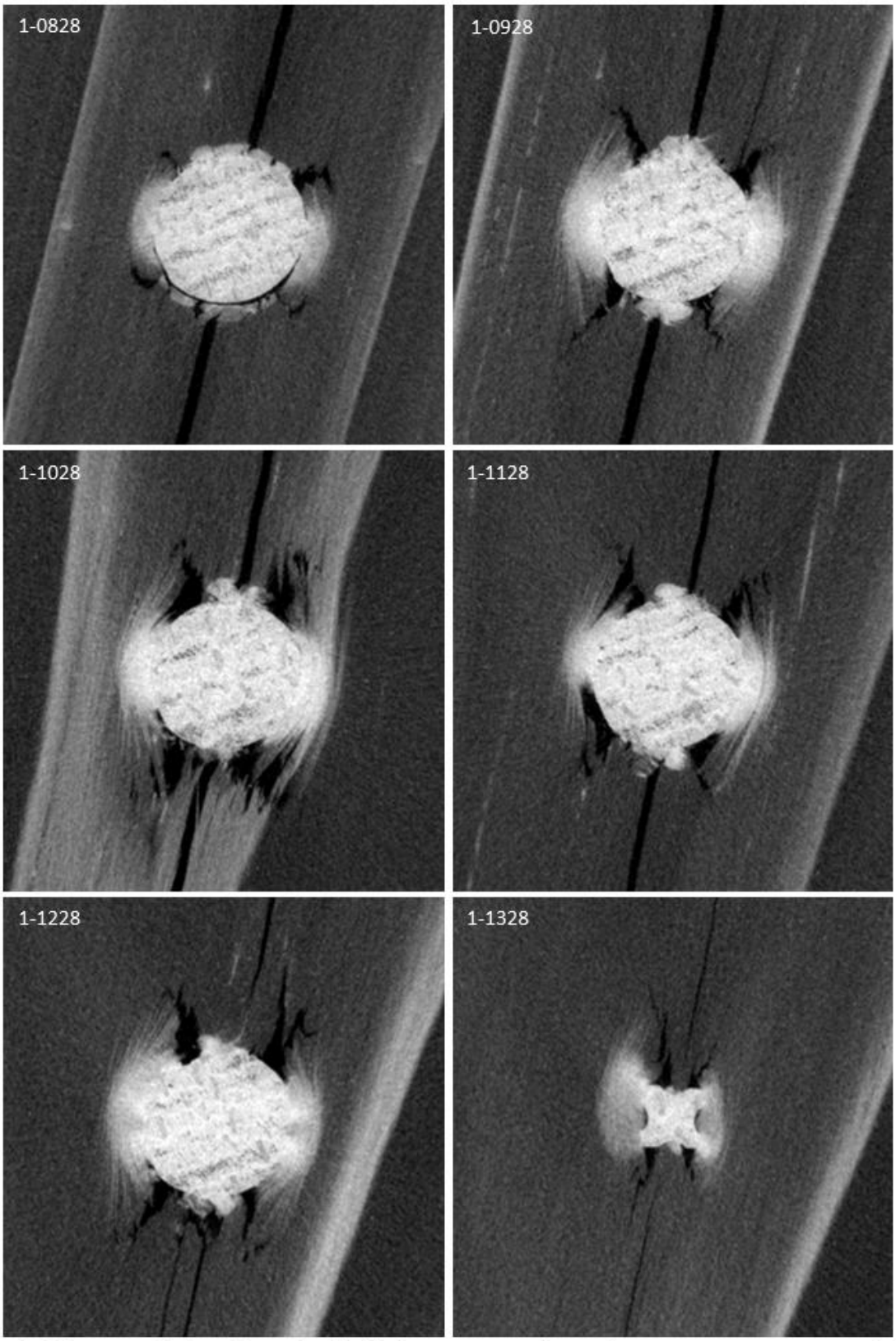


Fig. 9 CT images of a Lignoloc nail embedded in spruce wood, viewed in successive cross-sectional planes. Starting at the top left (1-0828) at the point of entry into the matrix, proceeding to the right and downwards in 100-voxel increments to the X-shaped tip of the nail (1-1328).

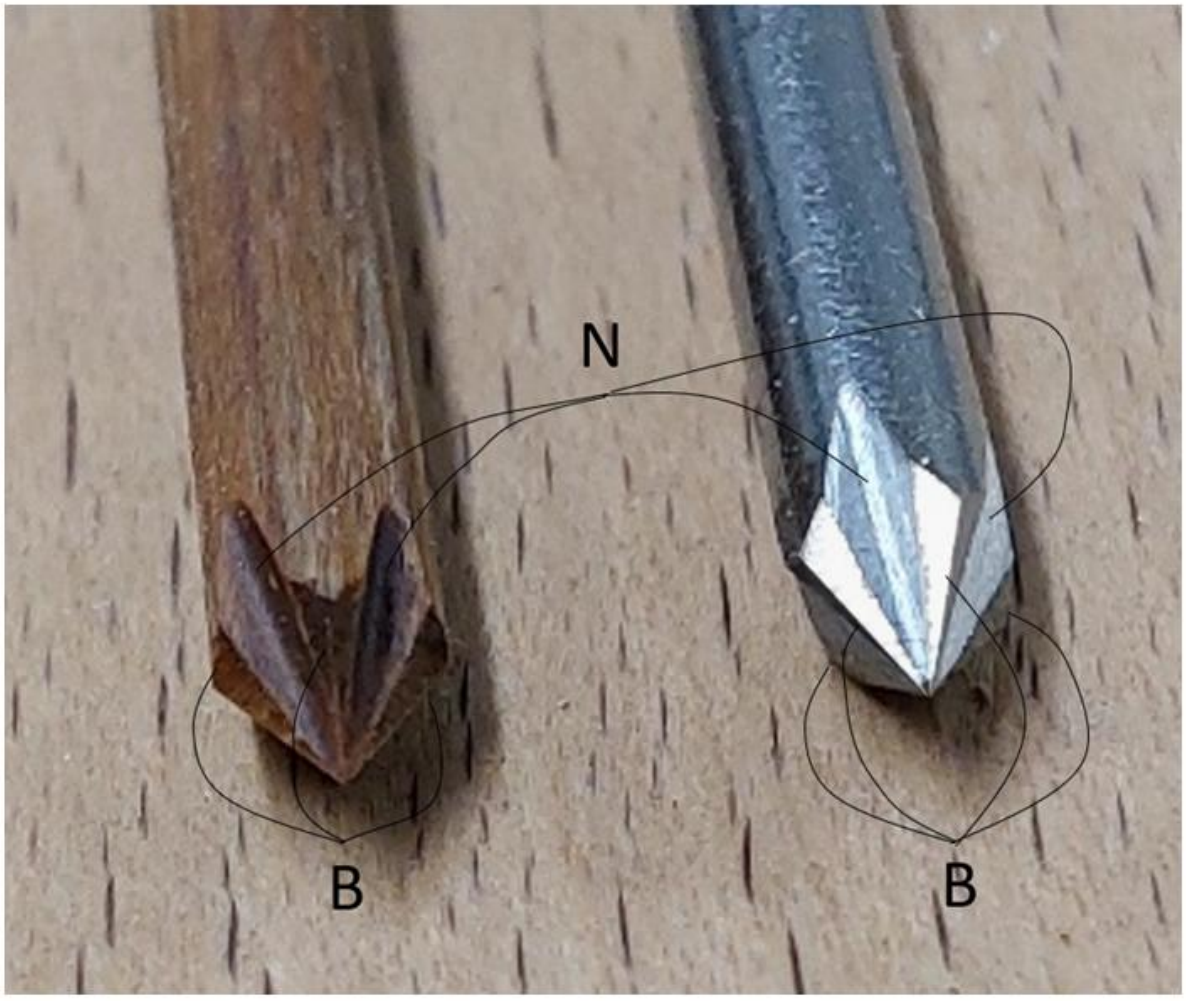


Fig. 8 Lignoloc (left) and steel nail (right) with a "Phillips"-tip and cutting sharp blades (B) between the notches (N).

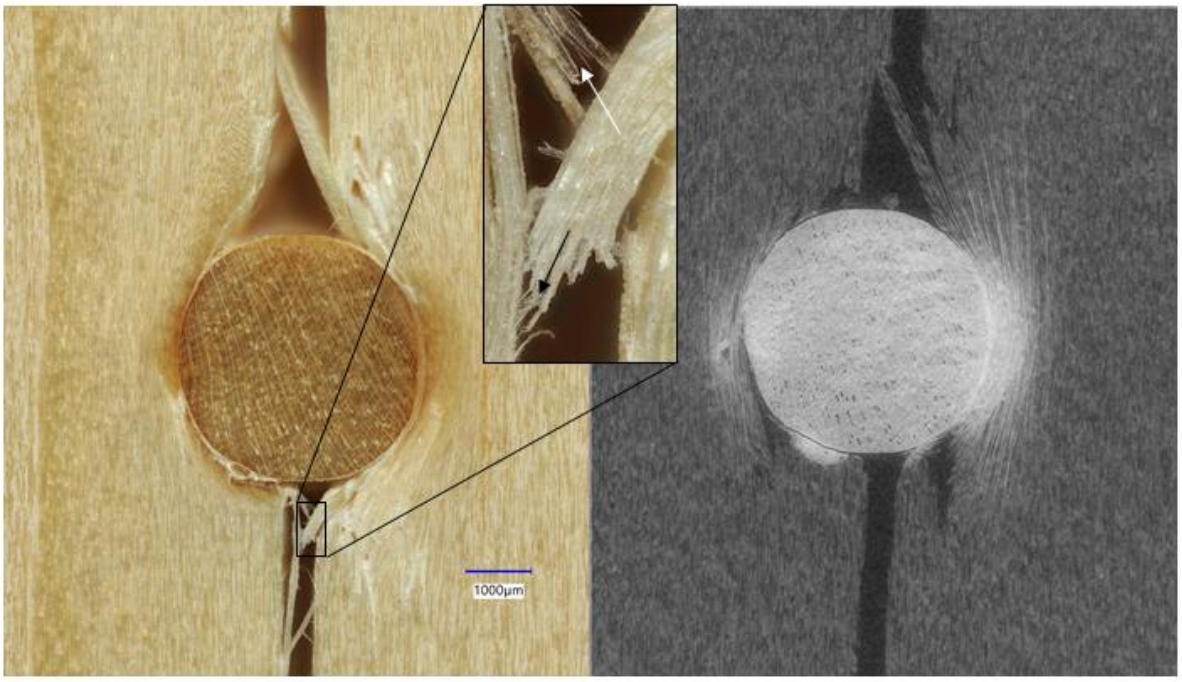


Fig. 7 Comparison of reflected light microscopy (left) and CT (right) of about the same region of an inserted hornbeam nail shot radially into spruce. Single fibres of fibre strands of spruce with tensile fracture tips (arrows).

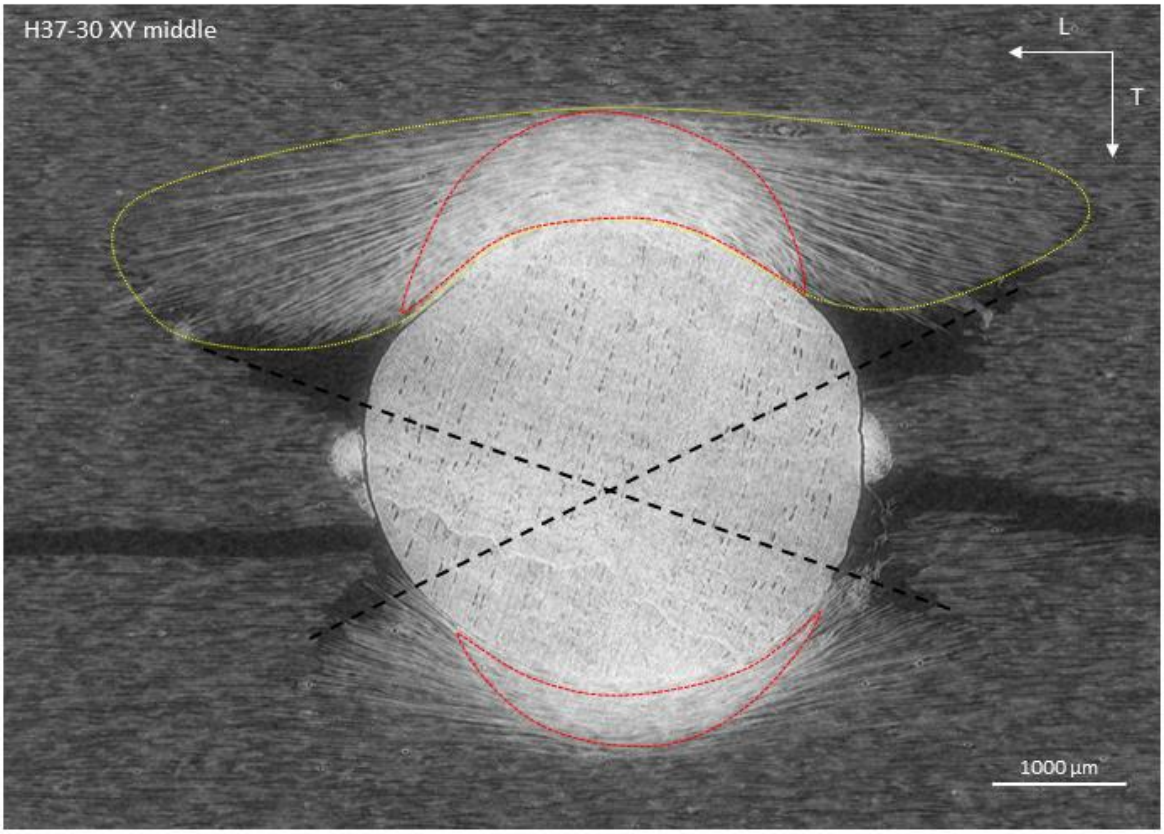


Fig. 6 CT image in the T/ L plane of a hornbeam nail (3.7 mm) in spruce matrix. Domes of densified spruce matrix are outlined in red, square ditted line. A densified dome is accompanied by slightly densified fibre strands which in some cases show tensile fractures. Together they have the form of a 'moth wing' (yellow, round dotted line). Black, dashed lines pronounce the X-shape of 4 triangular cracks.

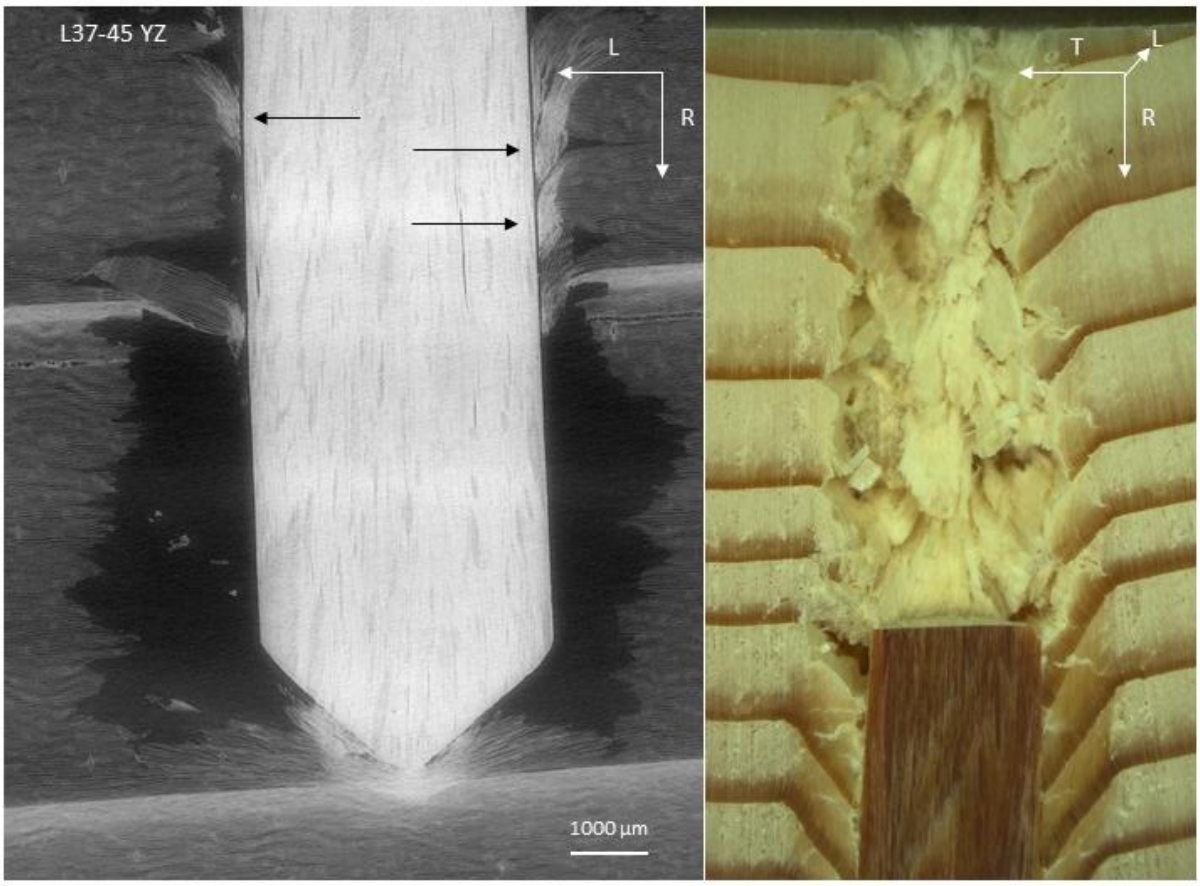


Fig. 5 (Left) CT image of the R/L plane of a Lignoloc nail (Ø 3.7 mm, tip angle 90°) in spruce. To the right and left of the nail, hollow areas caused by cracks (black areas) can be seen. Black arrows show bent earlywood fibres which are densified longitudinally. (Right) Reflected light microscopy with Keyence VHX-7000 of a shot channel in the T/R plane in spruce with a radially driven in nail some mm below the surface.

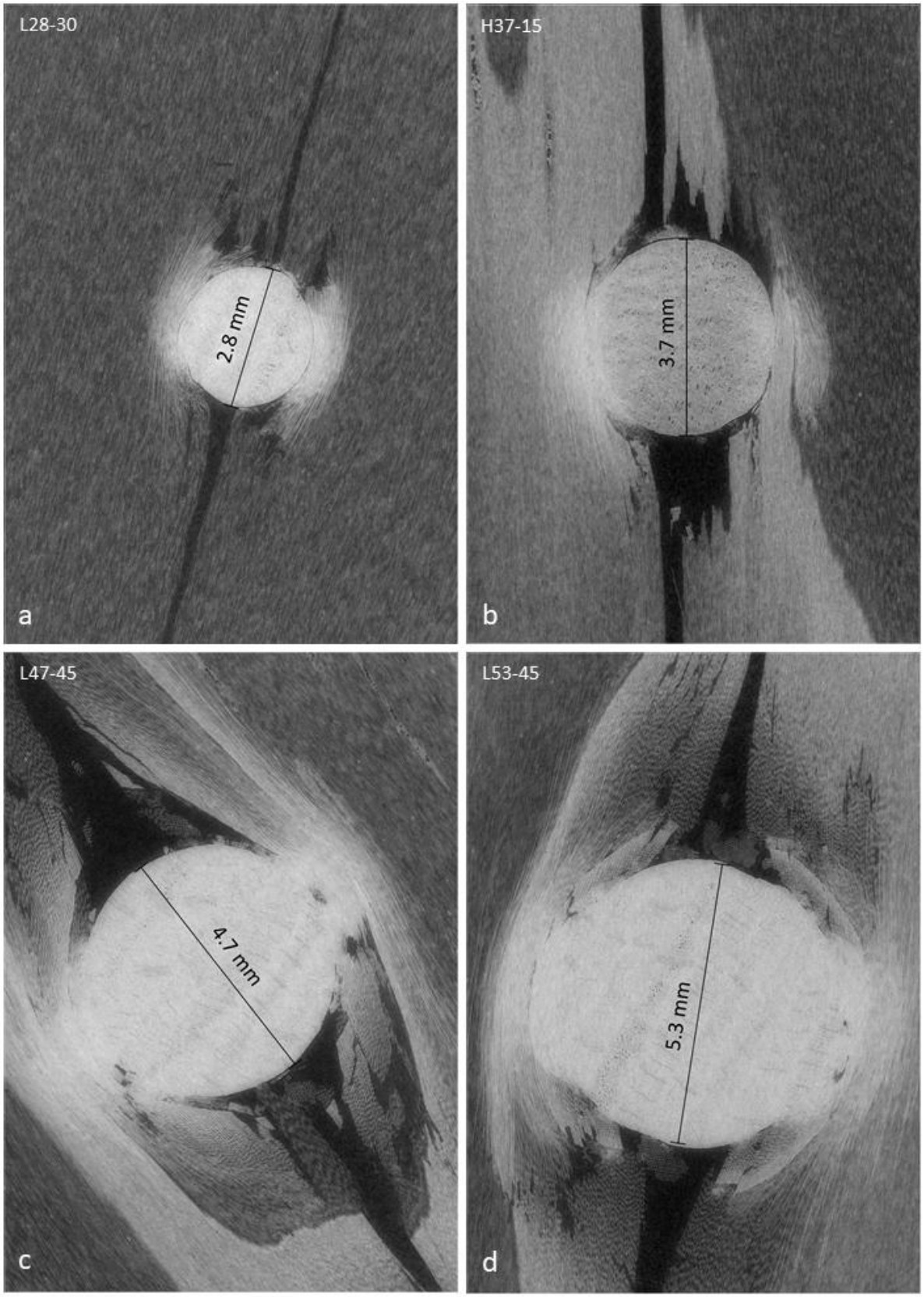


Fig. 4 Computer tomography (CT) images of hornbeam nails and Lignoloc of different diameters. a) Lignoloc 2.8 mm, b) Hornbeam 3.7 mm, c) Lignoloc 4.7 mm, d) Lignoloc 5.3 mm

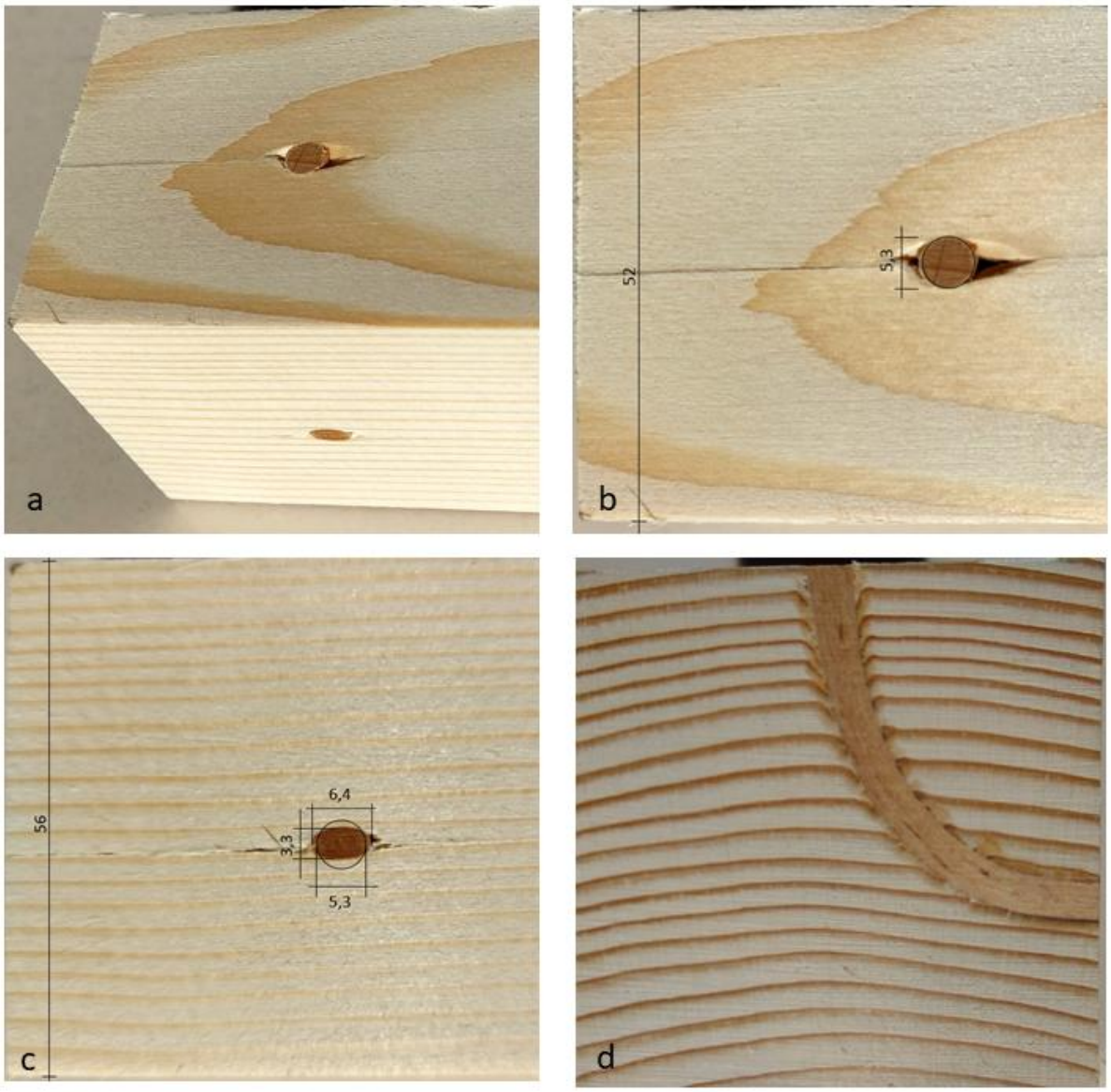


Fig. 3 Spruce with driven in and bound beech wood nail which is compacted to its front side. a) general overview of shot in T/L-plane (upper side) and rectangular R/T-plane (lower side) where the nails tip leaves the timber, b) detail of a) showing, that the cross section of the nail is circular and c) showing that the cross section becomes elliptical. d) Cross sectional view of the spruce matrix with 90° bound beech wood nail.

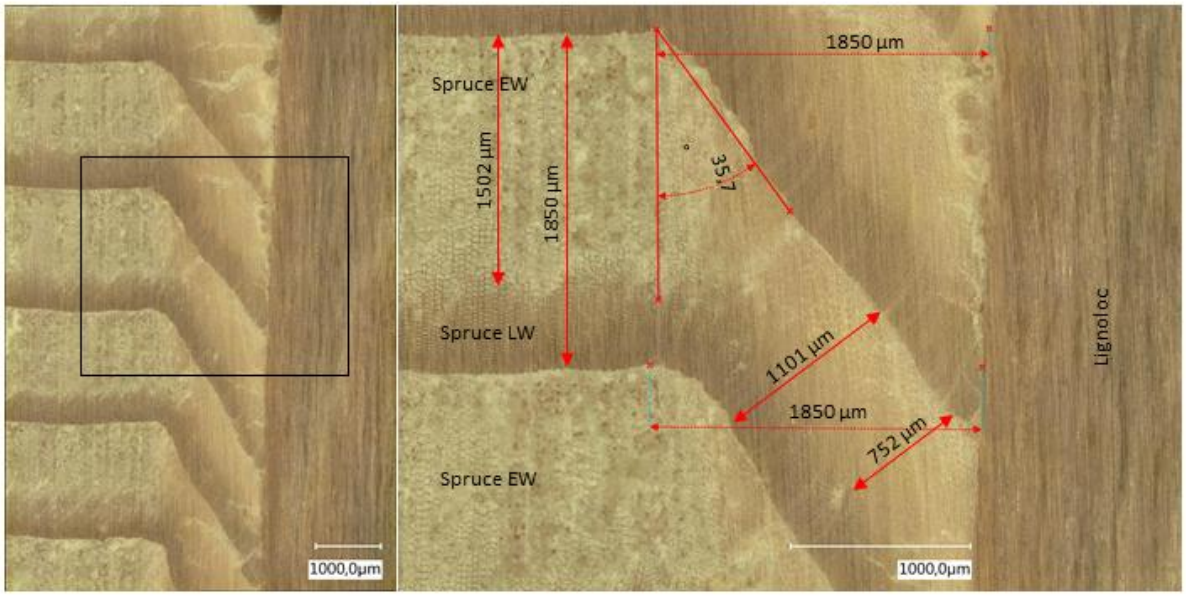


Fig. 2 Reflected light microscopy with Keyence VHX-7000 of a section of a Lignoloc nail embedded in spruce wood. Left side with frame cut-out, right side with enlarged frame in which the annual rings are measured. EW = early wood, LW = late wood.

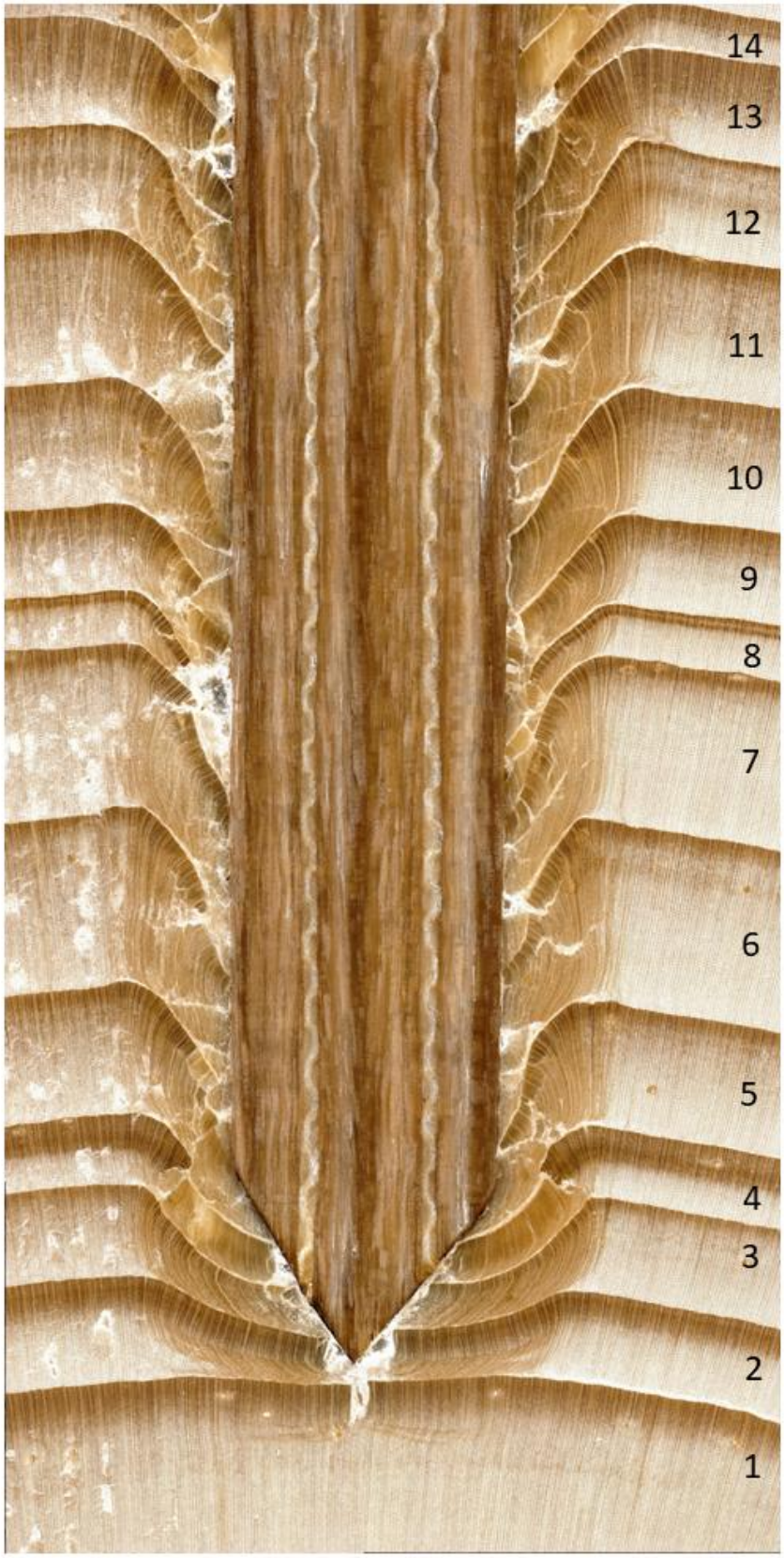


Fig. 1 Bent and compressed cell structures alongside a 3.7 mm diameter Lignoloc nail shot into spruce in radial direction. Right hand annual rings are numbered button up. Viewing plane is R/T.

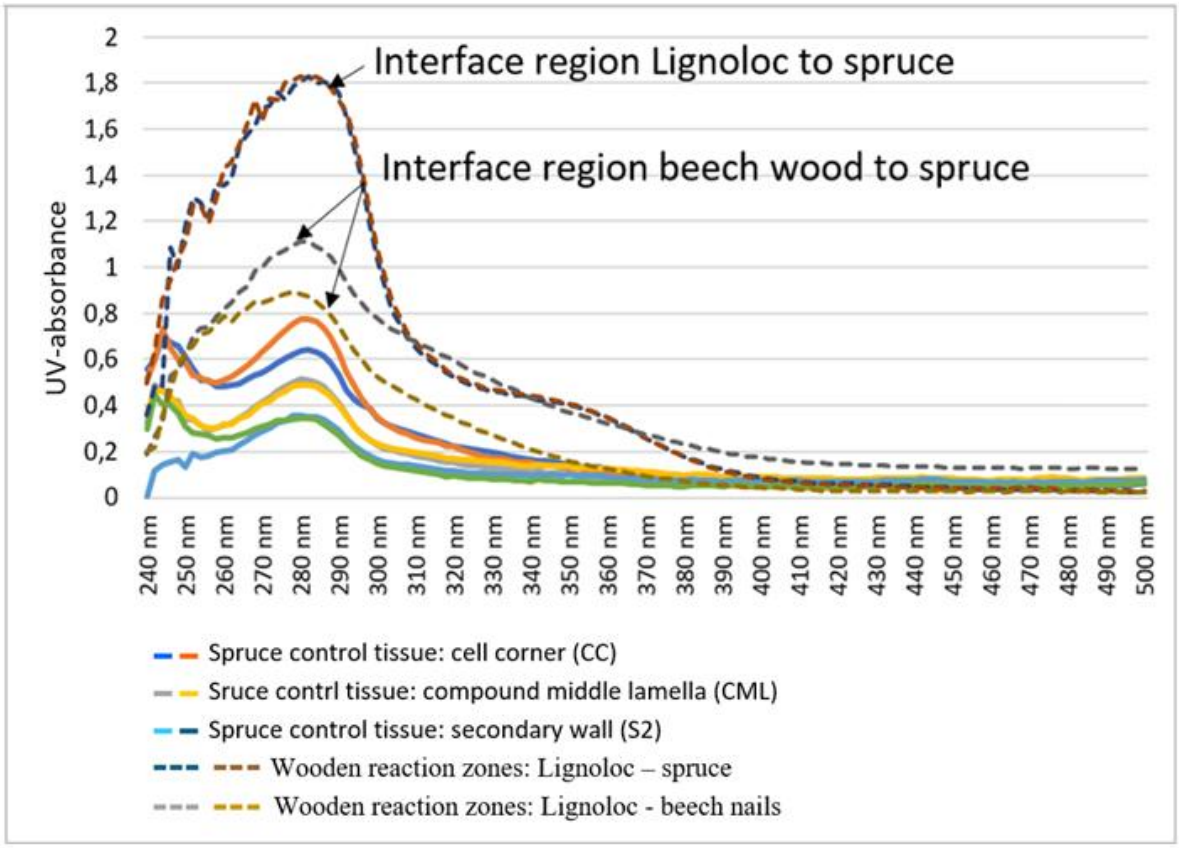


Fig. 16 Representative UV absorbance spectra of individual cell layers: cell corners (CC), compound middle lamella (CML) and secondary walls (S2) of spruce control wooden tissue in a wavelength range from 240 to 500 nm and wooden tissue in the reaction zones of Lignoloc and beech wood nails driven into spruce tissue.

Tab. 1 Side-chain lengths of the pyrolysis products (G-lignin building blocks) and their ratios in spruce wood, scraped fibres, Lignoloc (WN reference) and hornbeam (HBN ref.) nails. SC = Short Chain, LC = Long Chain, ΣG = Sum of all G-lignin building blocks, SD = Standard deviation

	matrix reference			matrix layer on nail surface						WN reference		HBN	interface
	spruce	spruce	spruce	⌀ 5.1	⌀ 5.0	⌀ 4.9	⌀ 4.8	⌀ 4.7	⌀ 4.6	total	tip	ref.	
Sample	**N98-107**	**N76-B**	**N94 [a]**	**N41**	**N43 [a,b]**	**N45**	**N49 [a]**	**N51**	**N53**	**N1**	**N59**	**N9**	**N97**
SC/ΣG	25%	20%	20%	24%	48%	25%	29%	28%	35%	37%	33%	22%	23%
SD	0%	2%		2%		2%		6%	3%	1%	2%	1%	1%
LC/ΣG	19%	15%	15%	10%	14%	8%	12%	12%	11%	11%	9%	9%	13%
SD	0%	1%		1%		1%		0%	1%	0%	2%	0%	0%
SC/LC	**1,3**	**1,4**	**1,4**	**2,4**	**3,4**	**3**	**2,4**	**2,4**	**3,2**	**3,3**	**3,6**	**2,4**	**1,7**
SD	0,05	0,03		0,36		0,28		0,52	0,50	0,01	0,60	0,13	0,13

[a] single analysis, [b] low extract amount analysed